BLADE PRESSURE DISTRIBUTIONS DURING SURGE OF A LOW-SPEED AXIAL-FLOW COMPRESSOR

by

Clifford Thomas Jones

Thesis submitted to the Graduate Faculty of the
Virginia Polytechnic Institute and State University
in partial fulfillment of the requirements for the degree of

MASTER OF SCIENCE

in

Mechanical Engineering

APPROVED:

H. L. Moses

W. F. O'Brien, Jr.

W. C. Thomas

August, 1977

Blacksburg, Virginia

ACKNOWLEDGMENTS

The author expresses his appreciation to those professors who served on his advisory committee: , Chairman, , and . The suggestions of in design of the experiment and the assistance of in instrumentation are especially appreciated.

The author thanks his wife, for her support and understanding during his year as a graduate student and for her excellent typing of this thesis.

TABLE OF CONTENTS

LIST OF TABLES

LIST OF FIGURES

NOMENCLATURE

a	speed of sound in air
A	area ratio
A_1	cross-sectional area upstream of nozzle
A_2	cross-sectional area of nozzle throat
A_c	compressor annulus area
A_p	plenum piston area
A_t	exit duct cross-sectional area
B	nondimensional compressor system parameter
C_1	absolute velocity upstream of rotor
C_2	absolute velocity downstream of rotor
C_c	axial velocity through compressor
C_t	axial velocity through exit duct
C_{w_1}	whirl velocity upstream of rotor
C_{w_2}	whirl velocity downstream of rotor
C_x	axial velocity component
E	nondimensional flexible plenum parameter
F	nondimensional flexible plenum parameter
g	acceleration of gravity
G	nondimensional compressor system parameter
H	nondimensional flexible plenum parameter
I	fraction of fixed plenum volume
J	nondimensional flexible plenum parameter
k	spring constant
K	flow coefficient

L_c	length of inlet duct
L_t	length of exit duct
$\dot{m}_c$	mass flow rate through compressor
m_p	mass stored in plenum
$\dot{m}_t$	mass flow rate through exit duct
M	mass of piston
n	integer exponent
N	number of rotor revolutions
P	static pressure
P_1	upstream static pressure
P_2	downstream static pressure
P_a	atmospheric pressure
P_c	pressure rise across compressor
P_{cs}	steady-state pressure rise across compressor
P_d	pressure difference due to centrifugal effects
P_o	stagnation pressure
P_{or}	stagnation pressure relative to rotor
P_p	plenum pressure
P_t	pressure drop across throttle
Q	volumetric flow rate
R	rotor blade tip radius
t	time
U	rotor blade velocity
V	fluid velocity
V_1	relative velocity entering rotor
V_2	relative velocity leaving rotor

V_p	plenum volume
$\overline{V}_p$	fixed plenum volume
x	piston displacement
α_1	absolute flow angle entering rotor
α_2	absolute flow angle leaving rotor
β_1	relative flow angle entering rotor
β_2	relative flow angle leaving rotor
γ	specific heat ratio
ρ	fluid density
ρ_p	plenum fluid density
τ	time constant
ω	Helmholtz resonator frequency

INTRODUCTION

The operation of an axial-flow compressor, as the throttle is closed from full flow, is characterized by an increase in pressure rise up to a local maximum at a moderate mass flow. As the flow is further reduced beyond this maximum, the rotor blades become stalled. This stall results in a reduction in compressor performance and a lower pressure rise across the compressor.

At some mass flow less than or equal to the stall point, the compressor begins to operate in an unstable mode. This instability can take on one or a combination of two forms, rotating stall and surge. Rotating stall is characterized by one to several cells of low flow rotating around the rotor in the opposite direction of rotor rotation, at a fraction of the rotor velocity. Surge is characterized by a cyclic discharging and charging of the plenum with an associated decrease and increase in mass flow through the compressor. If the surge is violent enough the compressor mass flow may even become negative. The form of instability which a compressor exhibits is determined by the system in which it is installed.

In applications where a compressor is required to operate over a range of mass flow rates, the possibility exists for the compressor to reach its instability point. It is desirable to know what form this instability will assume, since the method of return to stable operation depends on the mode of instability. During rotating stall, a hysteresis loop requires the mass flow rate to be increased beyond the instability point before the compressor can return to stable operation.

The surge cycle passes along a stable segment of the operating curve during a portion of the time, allowing for the possibility of return to stable operation without large changes in the throttle.

Operation of a high-speed compressor in the region of surge or rotating stall places the blades under severe dynamic loads. These dynamic loads can result in a catastrophic destruction of the machine by fatigue if it is allowed to operate under such conditions for extended periods of time.

In applications of high-performance compressors such as jet engines, where off-design operation is required, it is desirable to design the compressor for a wide range of stable operation. This flexibility is necessary to provide for rapid acceleration and insensitivity to inlet distortion.

From the previous discussion it is evident that two areas of study are necessary to meet these demands placed on the designer. One area of research should include a method of predicting the instability point and mode of instability, given the compressor characteristic and the geometry of the system in which it is installed. The other area should involve a detailed study of the actual flow through the compressor blades at the inception of the instability and during the instability cycle. Information from these studies will give the designer a better understanding of what causes surge and how compressors can be better designed to prevent it.

The work presented here includes an empirical study of the rotor blade pressure distribution during the surge cycle of a low-speed axial-flow compressor, as well as the cycle itself. An analytical

model for the stability of a typical compressor system is presented and applied to the system used in the experimental study.

LITERATURE REVIEW

The problem of surge in continuous-flow compressors has been recognized since the first applications of centrifugal compressors as superchargers. The earliest attempts to predict surge involved determining if the system was stable for a small deviation in mass flow. The models used were simplified to include only linear terms. More recently, with the availability of digital computers, nonlinear analyses of compressor systems have been used to predict the instability point as well as the mode.

The study of flow through compressor blades has been limited basically to cascade arrangements and steady mass flow across the blade row. Until recently the availability of on-rotor, blade pressure distributions was limited.

A NACA report on surge in centrifugal compressor systems by Bullock, Wilcox, and Moses [1]* gives experimental results of a parametric study, and a theoretical model for prediction of the surge point. Their experimental results give a qualitative idea of the effects of system geometry on the form of surge. The analytical model is simplified to include only linear terms. A small flow disturbance is assumed and the attenuation or amplification of the disturbance determines the system's stability.

Binder [2] presents a mathematical model for one type of surge. It is based on vibrations of a fluid in a pipe. When the compressor

---

*The numbers in brackets refer to list of references at end of thesis.

pressure rise increases with an increase in mass flow, there is a possibility for surge to occur. A critical condition exists when the pressure wave is in phase with the velocity wave.

Pearson and Bowmer [3] give a mathematical model of surge based on the inertia, capacity, and resistance of a compressor system. An electrical analogy is formed to make an analysis of the system easier to handle. Their theory is easily extended to include multistage machines. Several criteria for a system instability implying surge are investigated and compared with the surge points in actual machines.

Pearce [4] gives a qualitative discussion of the character and cause of surge, and a method of predicting the surge point. It is based on the instantaneous slope of the throttle curve in response to a change in the system mass flow rate. He describes a method for experimentally determining the value of the instantaneous throttle slope.

A discussion of surge as applicable to operation of jet engines is presented by Bullock and Finger [5]. A more complete description of operating difficulties and design considerations associated with surge in jet engines is given by Foley [6].

Huppert and Benser [7] differentiate between progressive and abrupt stall. The surge due to progressive stall is called classical surge and results from system instabilities. This compressor characteristic is continuous. The surge due to abrupt stall is called limit cycle surge. This compressor characteristic is discontinuous and surge will result if the system damping is low enough to allow the unstable compressor operation to reach the unstalled portion of the

curve.

Pearson [8] extends the analysis of surge to apply directly to jet engines. His analysis has the flexibility to include changes in the system operation due to a variation in fuel flow. A perturbation method is used to determine the stability of the system. He presents evidence to support an assumption of quasi-steady operation of the compressor during surge. He also gives reasons for assuming no acceleration of the engine and choked turbine operation in the stability analysis.

Emmons, Pearson, and Grant [9] give studies of both rotating stall and surge. They offer a qualitative explanation for the mechanism of rotating stall. For surge, the compressor system is modeled as a Helmholtz resonator. This model yields a physical understanding of the form of oscillation, and it gives frequencies on the same order of magnitude but somewhat higher than experimental data.

Pearson [10] differentiates between two types of surge by linking each of them with a different type of stall. Mild surge is characterized by small-amplitude oscillations and may or may not occur at the inception of rotating stall, depending on the relative size of the plenum. Deep surge is characterized by large-amplitude oscillations and occurs at full-rotor stall. The compressor characteristic at this point coincides with the throttle curve and identically satisfies the criteria for surge suggested in earlier studies. This form of oscillation is also dependent on the plenum size. For plenum volumes below a critical value, only one oscillation occurs and stable operation will resume at the lower branch of the discontinuity.

Lubick and Wallner [11] present a study of surge in gas turbine engines. Their results indicate that each stage stalls independently as the compressor stall point is approached. In general the stalling will progress from the last to the first stages, but not necessarily in sequential order. The thrust of their study is to determine the effect of transient operation on the stability of the engine. They were able to model the transient operation of the compressor on an analogue computer quite accurately.

Howell [12] presents a method for determining the surge line of a multistage compressor. His mathematical model is similar to the electrical analogy of a compressor system used by Pearson and Bowmer [3]. He incorporates a method of determining the individual unique compressor stage characteristics, set forth by Pearson [13]. This allows the interaction between stages to be taken into account when determining the stability of a compressor system. The criteria for stability used by Howell differs from Pearson and Bowmer's, "zero impedance looking downstream," in that the stability of the entire system of equations is considered. Nonoscillatory divergence is assumed to correspond to surge.

Hubbert [14] presents a collection of studies on surge in compressors. This work includes a good qualitative discussion of the types and causes of surge. He reiterates some of the conclusions he presented in reference 7. A redefinition of the limit cycle surge is notable.

Kuhlberg, et al. [15] give preliminary studies of several models of dynamic simulation of multistage compressors. Each model is based

on the steady-state stage characteristics and an associated stage volume. The model proving most applicable uses governing equations based on continuity of mass flow and conservation of momentum. A model neglecting momentum experiences difficulty in entering the compressor characteristic with pressure rise as the independent variable. This difficulty is due to the function being double valued. A model considering conservation of mass, momentum, and energy gives results similar to the momentum-continuity model, but is more complex and lacks the flexibility of the other.

Willoh and Seldner [16] develop a mathematical model to predict surge due to transient operation of a compressor. Their simulation techniques are very similar to those of Lubick and Wallner [11]; however, stage temperature rise as well as pressure rise are considered, and a momentum balance is used to determine stage flow. As in previous work the analysis is based on steady-state stage characteristics and associated lumped stage volumes. An analogue computer is employed to determine the stability boundary of the system.

Corbett and Elder [17] present a series of mathematical models for predicting surge in an axial-flow compressor. These models range from a complex set of equations derived from a rigorous analysis of the system, to more elementary sets based on various simplifying assumptions. These models are studied to determine their accuracy in predicting the surge point of actual compressor systems.

Greitzer [18] utilizes a nonlinear model to predict the mode of instability a compressor system will assume when the throttle is closed beyond the range of stable operation. This model assumes a

system consisting of a compressor forcing fluid through an inlet duct into a plenum, and exhaust passing through a throttle into an exit duct open to atmosphere. The compressor is modeled as an actuator disk. A conventional throttle characteristic is assumed. The fluid in the inlet and exit ducts is lumped and isentropic compression is assumed to take place in the plenum. Transient operation of the compressor is based on the steady-state characteristic coupled with a time constant. This time constant is determined from the time for circumferential growth of stall cells. A nondimensional parameter based on the compressor speed and the system geometry was found to be critical in determining the mode of instability. This model also yields the path of operation the compressor will follow during an instability.

In an accompanying paper, reference 19, Greitzer presents a series of tests on a compressor, varying the geometry of the system and the speed of the compressor. He uses a new method of data analysis allowing the determination of the instantaneous compressor operation during surge. The character of unstable operation predicted by the theoretical model compares very well with the experimental results. The theoretical numerical value of the nondimensional system parameter separating the two modes of instability is comparable to that given by the empirical study.

Many studies of flow through stationary cascades have been performed. A limited number of investigations of steady flow over compressor rotor blades have been done. Notable among these is a study by Schultz [20] in which a scanning valve was used to monitor rotor

blade pressure distribution during steady compressor operation. This equipment allows sequential monitoring of each pressure port. The availability of this equipment, as installed on the research compressor to be used, is vital to the study presented here.

EXPERIMENT

The objective of this experiment was to obtain the rotor blade pressure distribution of a low-speed axial-flow compressor during surge and to correlate these measurements to the corresponding point in the surge cycle. A comparison of the rotor blade pressure distribution during surge with the steady-state distribution was also made. To better understand the operation of the compressor as it was being tested, the steady-state compressor map was experimentally obtained. The experimental equipment, procedure, data acquisition and evaluation, and results are described in this section.

Equipment

Axial-Flow Compressor

The compressor used in this experiment is a General Electric Model Number 5GDY34A1. The compressor is driven by a directly-coupled 5.5-kW DC cradled dynamometer. This compressor is a research type with variable geometry, but the geometry as described below was held constant during the entire experiment.

The compressor is normally two-staged but was operated as a single-stage machine during this experiment. There is one stator section which functions as inlet guide vanes and one rotor. The inside casing diameter is 45.72 cm (18.00 in.), and the hub diameter is 31.43 cm (12.38 in.). There are 37 inlet guide vanes of circular-arc cross section. The guide vane mean radius stagger angle is 16 degrees, and the blades are twisted 8 degrees from hub to tip. The turning angle is

opposite that of rotor rotation. The rotor has 24 blades with RAF #6 cross sections. Coordinates for this airfoil as given by reference 21 appear in Table 1 and the section is shown in Fig. 1. The rotor blade mean radius stagger angle is 60 degrees, and the blade twist is 4 degrees from hub to tip. The blades are 6.99 cm (2.75 in.) long with a nominal tip clearance of 0.16 cm (0.063 in.). During this experiment, the rotor speed was held constant at 2400 RPM.

Compressor System

The compressor is connected to a 1.81 m^3 (64.0 ft^3) cubic plenum by way of a 0.91 m (3.0 ft) long duct 45.72 cm (18.00 in.) in diameter. The plenum discharges through a throttling valve into a duct 50.17 cm (19.75 in.) in diameter and 3.66 m (12.0 ft) long. The exit duct exhausts to atmosphere through a nozzle with an area ratio of 0.246. The plenum was modified by replacing the rigid top with a 1.22x0.91 m (4.0x3.0 ft) latex rubber diaphram 1.6 mm (0.063 in.) thick. A 14.9-kg (32.9 lbm) mass was fixed on top of the diaphram in the center. The purpose of this modification was to increase the effective volume of the plenum, and it allowed the compressor to surge with a plenum only one fourth the volume normally required according to Greitzer [18]. A schematic of the system is shown in Fig. 2.

Pressure Scanner

The rotor blade pressures were measured with a pressure scanner, Scanivalve®, model number 36 TR, manufactured by the Scanivalve

Table 1. Coordinates of RAF-6 Airfoil

fraction of chord	ordinate
leading edge radius	0.100
0.025	0.410
0.050	0.590
0.100	0.790
0.200	0.950
0.300	0.998
0.400	0.990
0.500	0.950
0.600	0.870
0.70	0.740
0.80	0.560
0.900	0.350
trailing edge radius	0.080

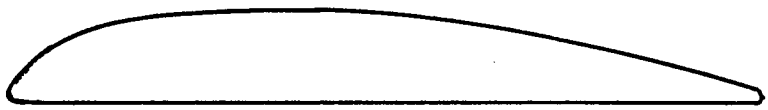

RAF - 6 12% THICKNESS/CHORD RATIO

FIGURE 1. ROTOR BLADE CROSS SECTION

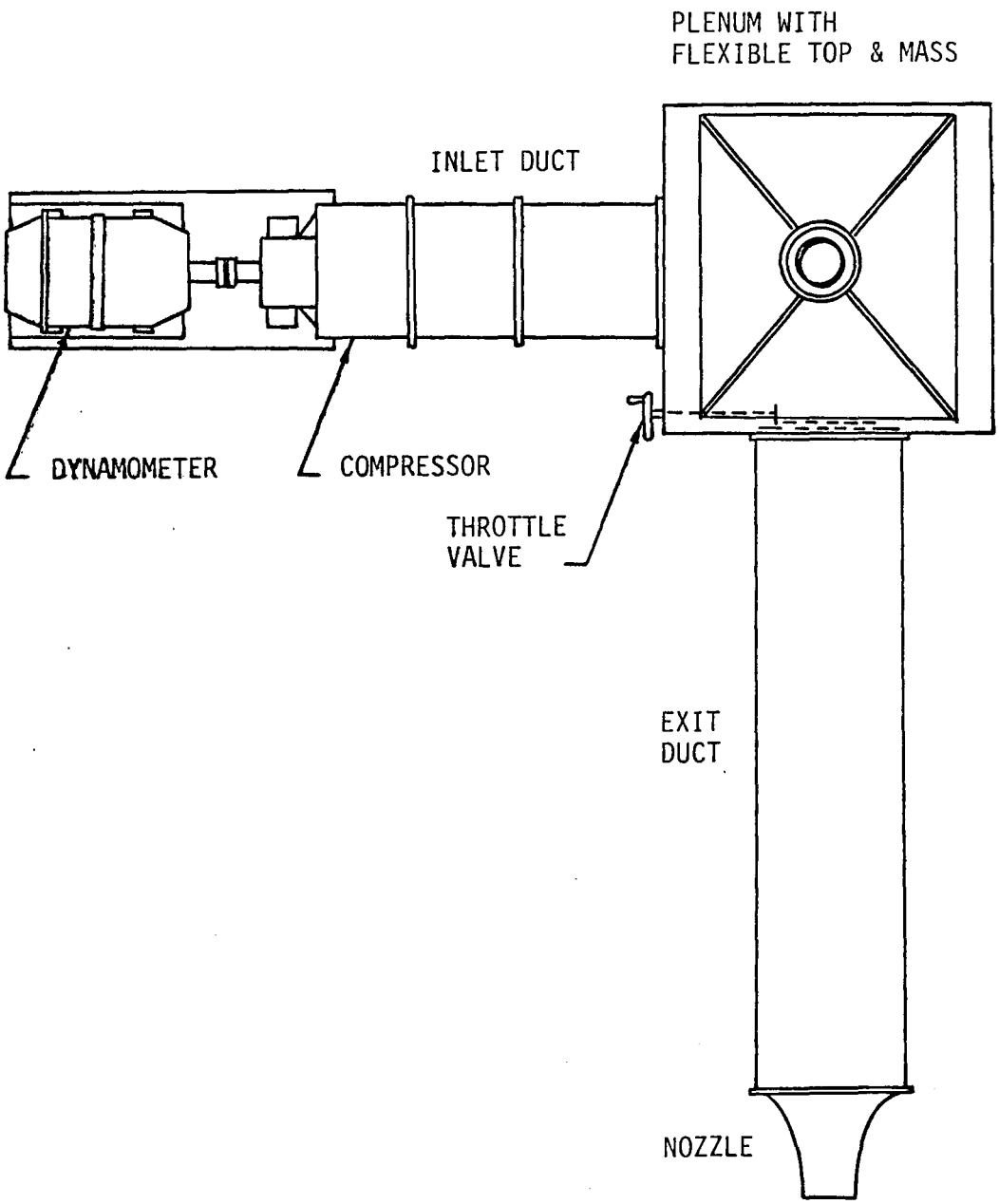

FIGURE 2. EXPERIMENTAL COMPRESSOR SYSTEM

Corporation, and henceforth referred to by its trade name. The 36 pressure ports which are available on the Scanivalve are attached to a rotating framework. Each port can be monitored sequentially by manually triggering an air-stepping motor. This motor changes the port that is connected to the single stationary pressure transducer, located on the axis of the hub. The pressure transducer was made by Druck Ltd., type PDCR 22, and has a range of 0-6.9 kPa (0-1.0 psi) and an output of 17 mV at 6.9 kPa (1.0 psi). Its linearity is within ±0.06% B.S.L.

Of the 36 pressure ports available on the Scanivalve only 31 are actually used in this system. Static-pressure ports are provided at five chordwise locations on each side of the blade. This is repeated at three different spanwise positions, accounting for 30 ports. A total-pressure port at the leading edge of the blade is also provided at one of the spanwise positions. The chord positions are 10, 25, 45, 65, and 85 percent chord. The span positions are 25, 50, and 75 percent span, the 50 percent position having the total-pressure tap. A picture of the installed Scanivalves is shown in Fig. 3.

To qualify the method of data acquisition for the on-rotor blade pressure distribution, the frequency response of the Scanivalve system was required. Such a test was made; the methods and results are reported in Appendix A.

Instrumentation

The compressor system was instrumented to monitor the inlet and

Figure 3. Photograph of the Scanivalve and the Rotor


TO EVEN

exit mass flow rates and the plenum pressure, as well as the blade pressures as described above. All parameters were sensed by transducers and available as electrical signals. The parameters were simultaneously available visually on an oscilloscope and also recorded on a reel-to-reel tape recorder.

The inlet velocity was sensed by a United Sensor pitot tube, model number PCC-12-KL. A Statham differential-pressure transducer, model number PM5TC ±0.15-350, was connected across the outlets of the pitot tube to convert dynamic pressure to an electrical signal. The pressure range of the transducer is ±1034.2 Pa (±0.15 psi). Restriction of flow in the pitot tube and the capacitance of the transducer limited the 99 percent rise time of the measuring system to 80 msec. This response time indicates a frequency response on the order of 3 Hz.

The exit mass flow rate was determined by the pressure drop across the exit nozzle. The static-pressure transducer is similar to that used with the pitot tube. The model number is PM5TC ±0.3-350 and the pressure range is ±2068.4 Pa (±0.3 psi). The response of the transducer is well above the range of interest.

The plenum pressure was sensed by a Statham pressure transducer identical to the one used to sense nozzle pressure drop.

The inlet velocity was also measured with a DISA Electronik constant-temperature hot wire anemometer, model number 55D01. The sensor is a DISA 0.13 μm tungsten hot wire, model number 55A22. The probe used is a DISA model 55A42. The signal output from the anemometer was linearized by a DISA linearizer, model 55D10.

The output of each transducer was amplified by a Honeywell

Accudata DC amplifier, model number 123. These amplifiers provide zero suppression, filtering and a range of gain from 0.05 to 5000. During this experiment, the zeros were not suppressed, the filtering on all signals was set to pass frequencies below 100 Hz, and the gains were individually adjusted to give output signals of one volt for the maximum expected signal.

The output of any two amplifiers could be visually monitored by a Tektronix storage oscilloscope, model number 564. The vertical amplifier had two channels and was a type 3A72. The time base was a type 2B67. A Tektronix scope camera, model C-12, was used to photograph selected storage displays.

The output of all amplifiers was recorded simultaneously on a 7-channel Ampex reel-to-reel FM recorder reproducer, model number 1300. A tape speed of 38.10 cm/sec (15.0 in./sec) was used during this experiment. This speed corresponds to a frequency response of 5000 Hz.

Procedure

The experiment consisted of three parts; measurement of the compressor map from shut-off to full flow, determination of the path of operation of the compressor during the surge cycle for a selected throttle position and measurement of the rotor blade pressure distribution during this surge cycle and during steady-state operation of the compressor at the same throttle setting. Each of these parts is discussed below in the order mentioned.

Steady-State Compressor Map

The steady-state pressure rise across the compressor was taken as the plenum pressure and was measured with an inclined water monometer. The pressure drop across the exit nozzle was measured with another inclined monometer. This pressure drop was used to determine the mass flow rate according to the expression,

$$Q = \frac{KA_2\sqrt{2(P_1-P_2)/\rho}}{\sqrt{1-(A_2/A_1)^2}} \quad , \tag{1}$$

where Q is volumetric flow rate, K is a constant determined by the Reynolds number, A is cross-sectional area, P is static pressure, ρ is density of the fluid, and 1 and 2 refer to the upstream and downstream conditions respectively.

With the nozzle in place, the compressor is loaded too much to reach the full-flow portion of the map. The throttling valve is also designed so that it can never be completely closed. This situation makes it necessary to obtain the map in three separate segments. The portion of the throttle that remains open normally was blocked during the first test. This modification allowed the compressor to be operated from near shut-off to the middle portion of the map. This test was repeated with the throttle unblocked. The second test allowed more of the map to be determined and was used to obtain valve flow coefficients for each of the valve positions tested. With these valve flow coefficients available, the nozzle was removed to unload

the compressor and the flow through the throttle was determined from the plenum pressure. The shut-off pressure was found by merely blocking the exit duct.

During the tests, two Kulite high-response differential-pressure transducers, model number CQH-152-15D, designed to sense dynamic pressure, were located directly behind the rotor, near the tip, oriented in the axial direction, and 105 degrees apart. The signals from these probes were monitored on an oscilloscope as the compressor characteristic was measured. They indicated the point where the compressor entered rotating stall. In this compressor there was only one rotating stall cell. As the flow rate was further reduced full-rotor, part-span stall occured.

In reducing the data, plenum pressure and mass flow rate were nondimensionalized by $1/2\rho U^2$ and $\rho A_c U$ respectively, where ρ is ambient air density, U is rotor blade tip speed, and A_c is the compressor annulus area.

Surge Cycle

The entire surge experiment was done with the throttle setting held at position 3. This gave a mild surge of the limit cycle type due to a positively-sloped characteristic. The frequency of the surge cycle was 1.56 Hz. To determine the instantaneous operating point of the system, the mass flow rate and plenum pressure had to be determined as a function of time.

The mass flow rate was measured by recording the axial velocity

upstream of the inlet guide vanes at ten equally-spaced intervals between the 5 and 95 percent span positions. Pitot tube and hot wire signals were recorded simultaneously on the storage scope and photographed for each spanwise location. A similar traverse of the compressor annulus was made with the hot wire between the stator and the rotor. The pitot tube was fixed upstream of the stator at 50 percent span. Both signals were stored and photographed simultaneously. The pitot tube gave the cleanest signal and was used as a key to the relative point in time of the surge cycle during the entire experiment.

The plenum pressure corresponding to the instantaneous compressor mass flow rate was determined by simultaneously storing the plenum pressure and the pitot signal of the 50 percent span position. The exit mass flow rate signal was also stored and photographed with a simultaneous pitot signal at the same span position.

The instantaneous inlet mass flow rate was computed by numerically integrating the mass flux across the inlet annulus. The surge cycle was divided into eight equal time intervals of 0.08 sec each. The inlet mass flow rate was determined for each of these eight points in time. The hot wire signal upstream of the stator was used as the basis for determining the required velocities. The flow was assumed axial.

The data were consistently nondimensionalized by dividing plenum pressure by $1/2\rho W^2$, mass flow rate by $\rho A_c U$, and velocity by U.

Blade Pressures

The rotor blade pressure distribution during the surge cycle was determined by storing the pressure signal from each Scanivalve port and a simultaneous signal from the pitot tube on the oscilloscope. A photographic record of each pressure port and its key signal was made. During the entire test the pitot tube was positioned upstream of the stator and at the 50 percent span position. The rotor blade pressure distribution corresponding to the instantaneous compressor operating point was correlated by the pitot tube key signal. The time points evaluated correspond directly to those reduced in the surge cycle experiment.

The steady-state blade pressures were obtained by fixing a rigid cover over the flexible plenum top to maintain stable operation. A low-pass filter attenuating frequencies above 0.16 Hz was used on the output of the amplifier. The signal was read from a Keithley digital volt meter, model 168.

Each blade pressure port is connected to the Scanivalve by tubing mounted on the rotating framework. During operation, the centrifugal effect on the rotating column of fluid in each tube causes a pressure difference between the port location on the blade and the stationary pressure transducer located at the center of rotation. This pressure difference is given by

$$P_d = 1/2\rho U^2, \tag{2}$$

where d indicates centrifugal effect. The true blade pressures were obtained by adding P_d to the measured value.

The velocity triangles for this compressor are shown in Fig. 4. The absolute velocity of the flow C_1 leaving the stators was computed from the upstream axial velocity C_x measured in the surge cycle experiment, by

$$C_1 = C_x/\cos \alpha_1 \quad , \tag{3}$$

where α_1 is the turning angle of the inlet guide vanes. The velocity relative to the blade V_1 is given by

$$V_1 = C_x/\cos\{\tan^{-1}[\tan \alpha_1 + U/C_x]\} \quad . \tag{4}$$

Bernoulli's equation for incompressible flow gives the stagnation pressure P_o as

$$P_o = P + 1/2\rho V^2 \quad , \tag{5}$$

where P is static pressure and V is flow velocity. The stagnation pressure ideally remains atmospheric through the stators, therefore the static pressure entering the rotor P_1 is given by

$$P_1 = P_a - 1/2\rho C_1^2 \quad , \tag{6}$$

where a indicates atmospheric pressure. The total pressure relative

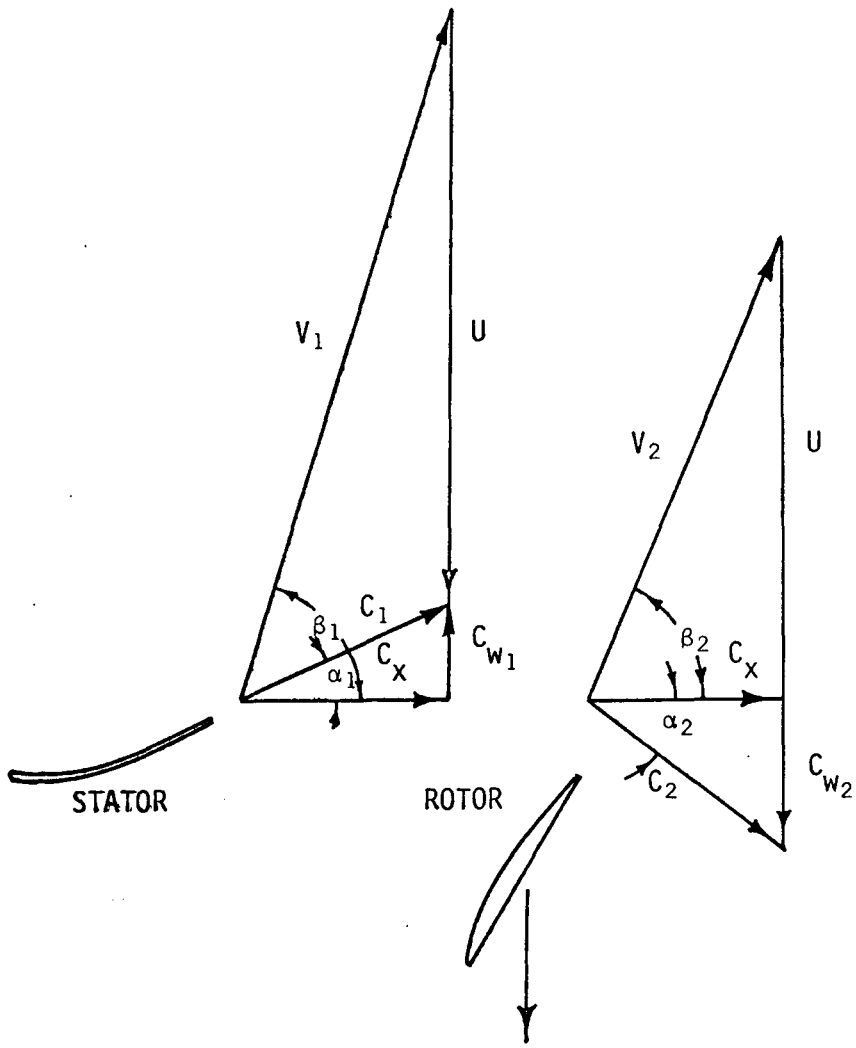

FIGURE 4. VELOCITY TRIANGLES

to the rotor P_{or} is then

$$P_{or} = P_a + 1/2\rho(V_1^2 - C_1^2) \quad , \tag{7}$$

Expressing the total pressure relative to the rotor in terms of the relative velocity and static pressure yields

$$P_{or} = P_1 + 1/2\rho V_1^2 \quad . \tag{8}$$

Since the total pressure through the blade passages remains constant except for losses, it can be rewritten in terms of the static pressure at the blade surface P and the local fluid velocity V relative to the rotor as

$$P_{or} = P + 1/2\rho V^2 \quad . \tag{9}$$

The rotor blade pressure distribution was nondimensionalized by subtracting the blade static pressure from the total pressure and dividing by the dynamic pressure at the leading edge of the blade. This yields

$$(V/V_1)^2 = (P_{or} - P)/(1/2\ V_1^2) \quad . \tag{10}$$

Experimental Results

The experimental steady-state compressor map with fixed plenum volume is shown in nondimensional form in Fig. 5. Closure of the

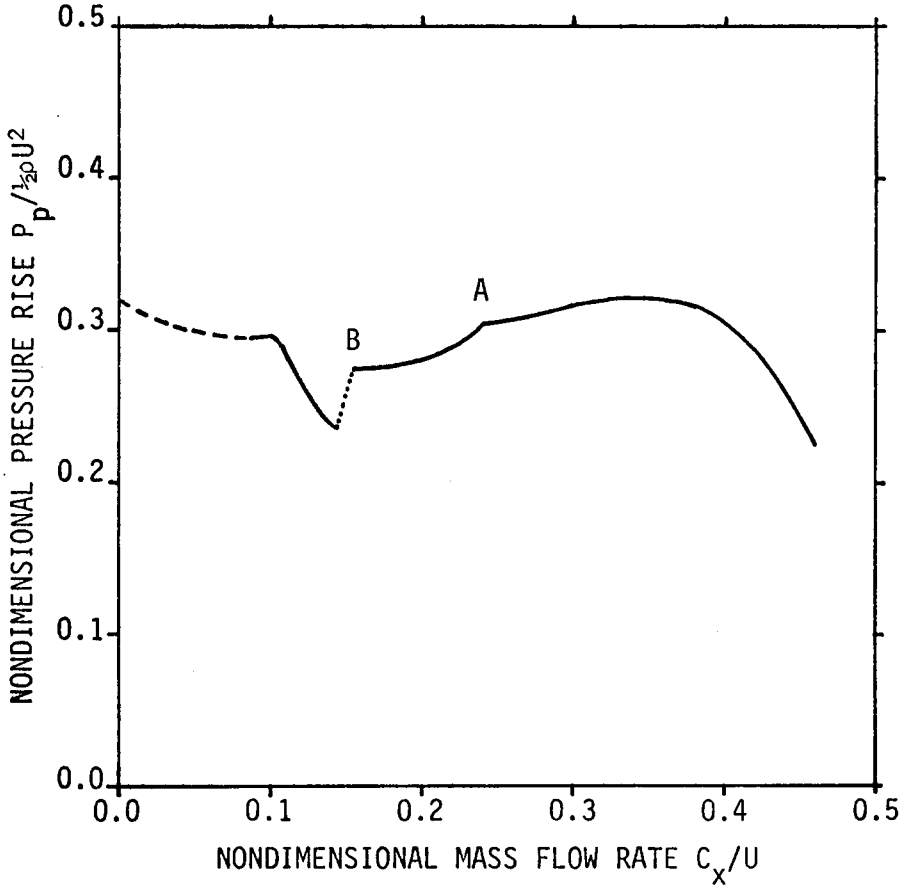

FIGURE 5. STEADY-STATE COMPRESSOR CHARACTERISTIC

throttle could not be accomplished gradually so a continuous dashed curve is fared between the minimum positive data point and shut-off. The portion of the curve over which data points were taken is shown as a solid line. Measurements were taken too close together to show discrete points. The dynamic-pressure probes indicated that the inception of rotating stall occured at point A. Rotating stall collapses to full-rotor, part-span stall at point B. At this point the compressor characteristic is discontinuous. This discontinuity is shown as a dotted line. The compressor exhibits some hysteresis when the throttle is opened from shut-off. The characteristic shown in Fig. 5 corresponds to the throttle being closed. The hysteresis curve follows this curve within 6 percent of the plenum pressure and is omitted for clarity. The plenum pressure and the pressure drop across the nozzle could be read within ±0.5 percent of the maximum pressure obtained. This data was repeatable within ±3 percent of the average value.

The nondimensional inlet velocity profiles upstream of the stators are shown in Fig. 6 for sequential equal intervals of time in the surge cycle. The solid lines represent the profile as it increases from minimum to maximum mass flow rate, and the dashed lines show the profile as the mass flow rate returns to its minimum value. The time interval between each profile is 0.08 sec. Velocity values obtained from the hot wire were read from the oscilloscope photographs. The minimum time graticule is 0.04 sec, so time could be read within 3 percent of the surge cycle period. The velocity could be read within 3 percent of the mean. Repeatability of the velocity trace was about

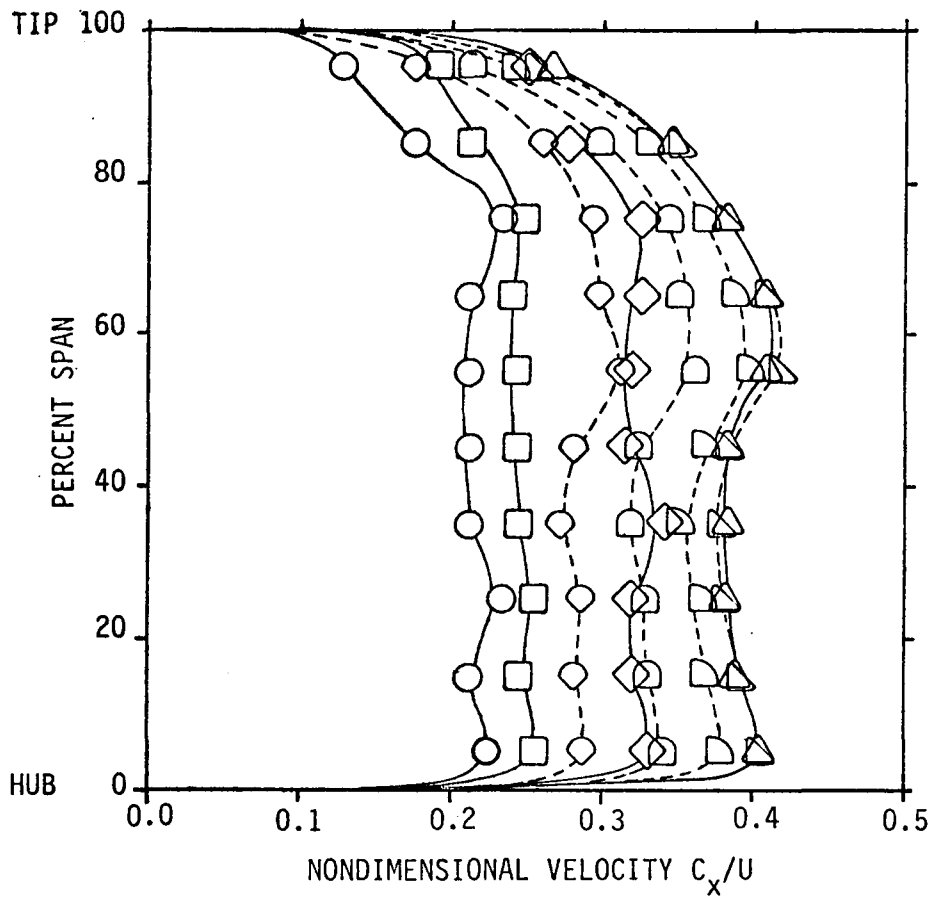

FIGURE 6. INLET VELOCITY PROFILE

HUB RADIUS/ TIP RADIUS = 0.69

SEQUENCE: ○□◇△◺◺▢◇

7 percent of the mean velocity. The presence of rotating stall is visible as regularly-occuring spikes about 50 msec apart as the velocity recovers from its minimum value. A very distinct spike occurs in the velocity as it starts to drop off from its maximum. In order to present the data in a meaningful form, means of the rotating stall cell velocity and the large spike velocity were used. Traces of the hot wire and pitot tube at mean span upstream of the stator are shown in Fig. 7.

The resolution of the plenum pressure on the photograph is 1 percent of the average pressure. The time base on the oscilloscope was held constant during the entire experiment, so the time resolution remains within 3 percent of the cycle period. Repeatability of the plenum pressure trace was about 7 percent also. The plenum pressure wave-form has an additional vibration superimposed on it. A best mean curve was fared through this fluctuation to make the surge cycle more meaningful. A trace of the plenum pressure and pitot tube, which is fixed at the 50 percent span during the rest of the experiment, is pictured in Fig. 7.

A plot of plenum pressure against mass flow rate indicating the path the surge cycle follows is shown on the nondimensional steady-state compressor map in Fig. 8. The data point symbols correspond to the same points in time of the cycle as they do in the velocity profiles in Fig. 6.

A picture of the pressure drop across the nozzle is shown in Fig. 9. It has a repeatability comparable to that of the velocity and plenum traces.

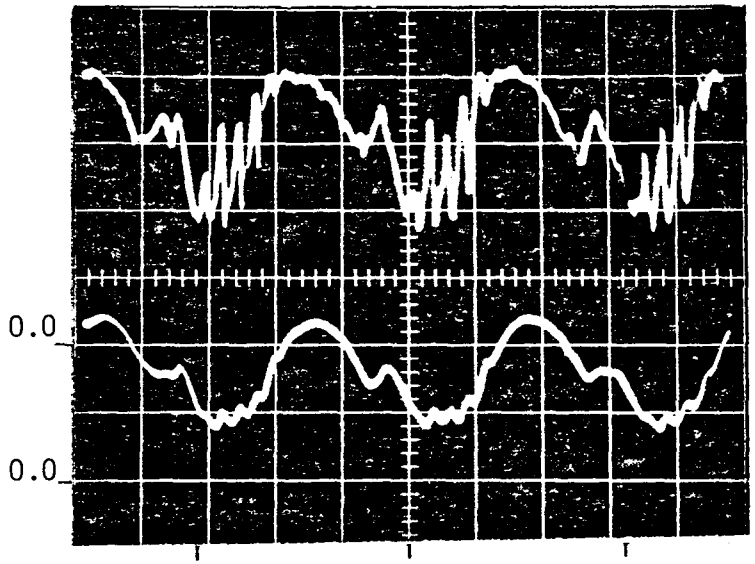

TICK MARKS INDICATE TIME OF MINIMUM FLOW RATE

VERTICLE AXIS:

TOP TRACE - HOT WIRE, VELOCITY
6.10 m/sec (20.0 ft/sec)
PER MAJOR GRATICULE
ZERO AT FOURTH GRATICULE

BOTTOM TRACE - PITOT TUBE, DYNAMIC PRESSURE
0.10 kPa (0.40 in. H_2O) PER
MAJOR GRATICULE
ZERO AT SECOND GRATICULE

HORIZONTAL AXIS: TIME, 0.2 sec PER
MAJOR GRATICULE

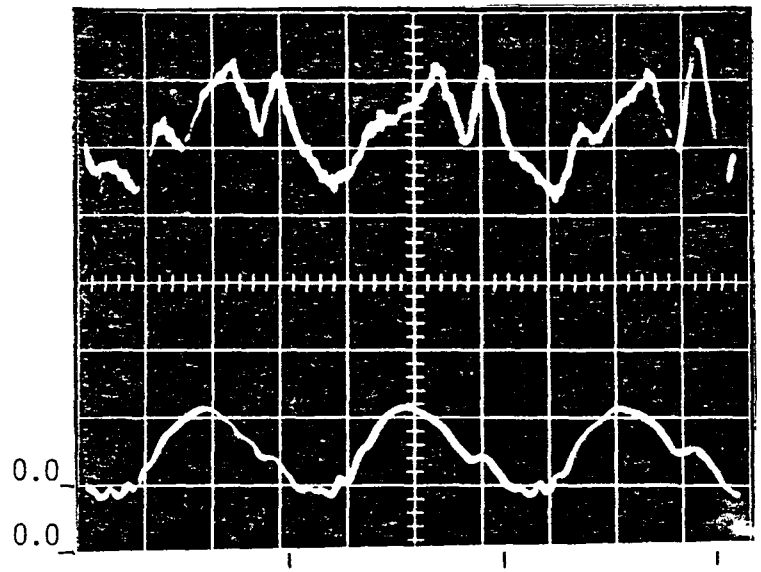

TICK MARKS INDICATE TIME OF MINIMUM FLOW RATE

VERTICLE AXIS:

TOP TRACE - PLENUM PRESSURE
0.10 kPa (0.40 in. H_2O)
PER MAJOR GRATICULE
ZERO AT SECOND GRATICULE

BOTTOM TRACE - PITOT TUBE, DYNAMIC PRESSURE
0.10 kPa (0.40 in. H_2O) PER
MAJOR GRATICULE
ZERO AT FIRST GRATICULE

HORIZONTAL AXIS: TIME, 0.2 sec PER
MAJOR GRATICULE

FIGURE 7. UPSTREAM HOT WIRE AND PLENUM PRESSURE TRACES

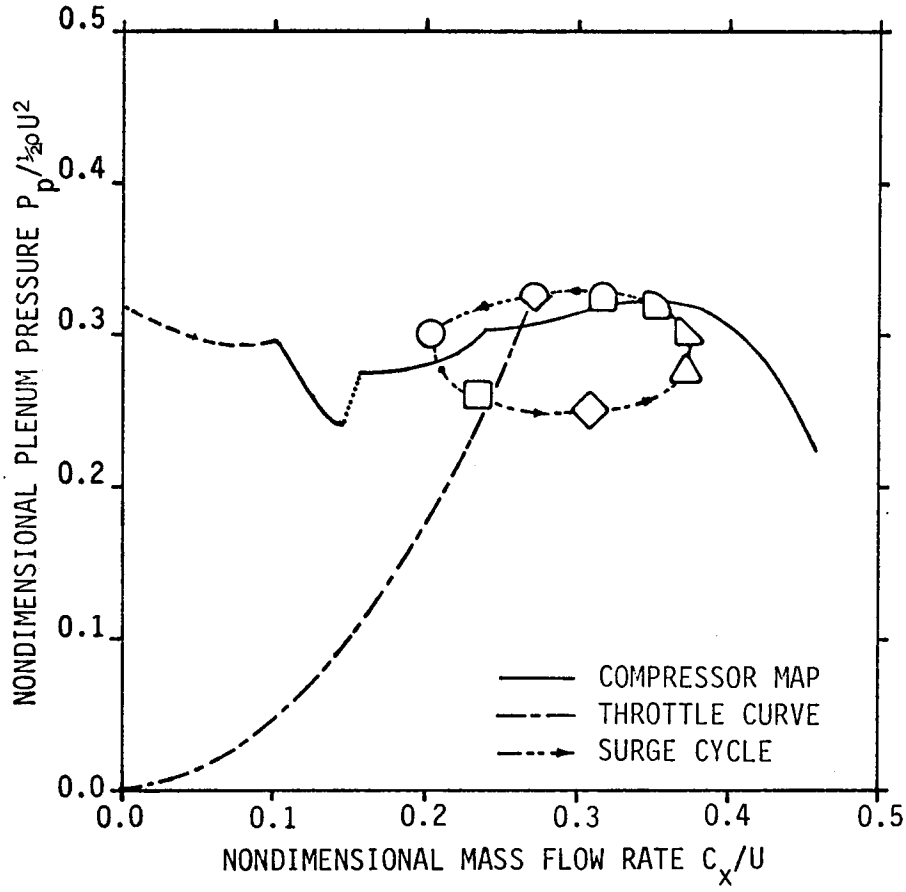

FIGURE 8. EXPERIMENTAL SURGE CYCLE

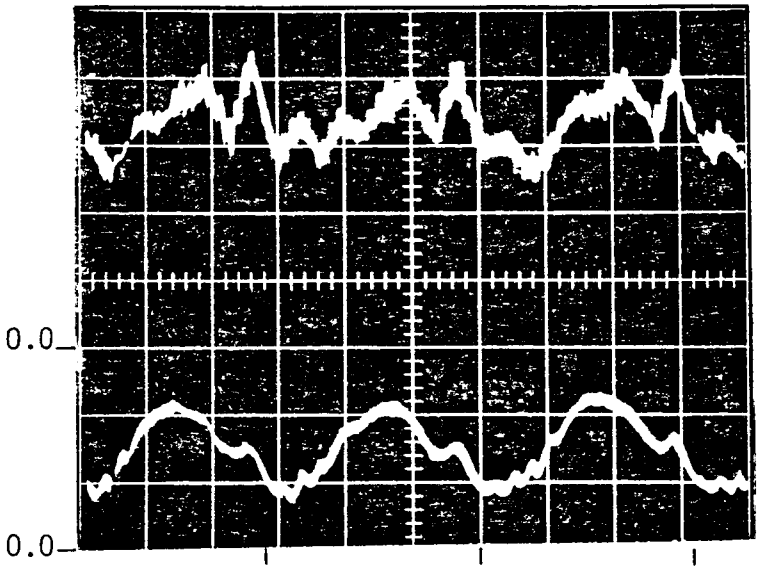

TICK MARKS INDICATE TIME OF MINIMUM FLOW RATE

VERTICLE AXIS:

TOP TRACE - NOZZLE PRESSURE DROP
0.10 kPa (0.40 in. H_2O)
PER MAJOR GRATICULE
ZERO AT FOURTH GRATICULE

BOTTOM TRACE - PITOT TUBE, DYNAMIC PRESSURE
0.10 kPa (0.40 in. H_2O)
PER MAJOR GRATICULE
ZERO AT FIRST GRATICULE

HORIZONTAL AXIS: TIME, 0.2 sec PER
MAJOR GRATICULE

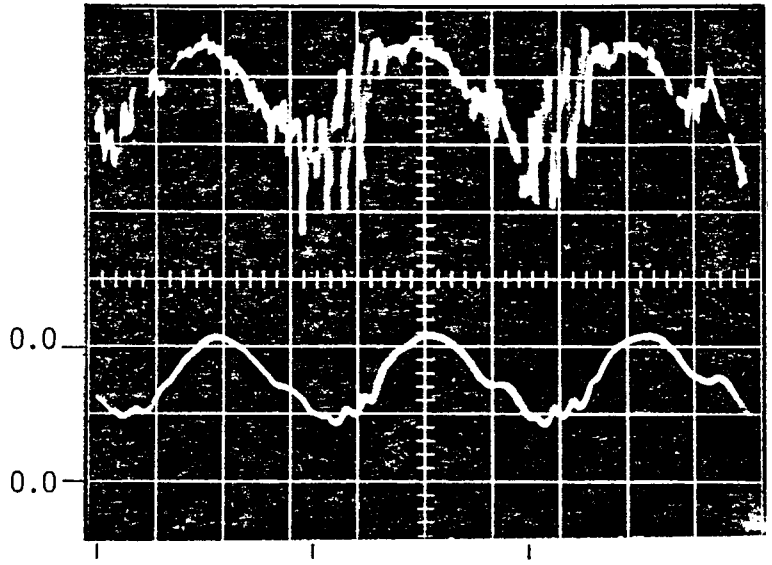

TICK MARKS INDICATE TIME OF MINIMUM FLOW RATE

VERTICLE AXIS:

TOP TRACE - HOT WIRE, VELOCITY
6.10 m/sec (20.0 ft/sec)
PER MAJOR GRATICULE
ZERO AT FOURTH GRATICULE

BOTTOM TRACE - PITOT TUBE, DYNAMIC PRESSURE
0.10 kPa (0.40 in. H_2O)
PER MAJOR GRATICULE
ZERO AT SECOND GRATICULE

HORIZONTAL AXIS: TIME, 0.2 sec PER
MAJOR GRATICULE

FIGURE 9. NOZZLE PRESSURE AND DOWNSTREAM HOT WIRE TRACES

During the traverse of the hot wire across the annulus between the stator and rotor it was oriented axially. This gives an indication of the character of the velocity but not a good quantitative estimate, since the guide vanes give the flow a swirl component. A picture of the hot wire signal at the mean span and the upstream pitot signal are given in Fig. 9.

The nondimensional rotor blade pressure distributions are shown in Figs. 10-12 for sequential equal intervals of time in the surge cycle. The data for each span position is presented in a pair of graphs. The "a" subscripted figures show the pressure distribution as the mass flow rate increases. The "b" subscripted ones correspond to decreasing mass flow. Each plotting symbol represents the same point in the cycle as it does in Figs. 6 and 8. The pressure distributions are given for the 75, 50, and 25 percent span in Figs. 10, 11, and 12 respectively. Resolution of the traces of the suction side of the blade is 4 percent of the maximum measured blade pressure value. The repeatability of these signals is about 5 percent of the mean pressure. The resolution of the pressure side traces is comparable to the criteria given for the suction side. The repeatability of the pressure side is equal to or better than the suction side. The traces from which the data was taken are presented in Figs. 13, 14, and 15 for the span positions 75, 50, and 25 percent respectively. The subscript "a" represents the suction side and "b" the pressure side. The time point corresponding to minimum flow rate is marked on each trace. This point corresponds to the circle data symbol. The total pressure at the blade leading edge for 50 percent span is shown in Fig. 16.

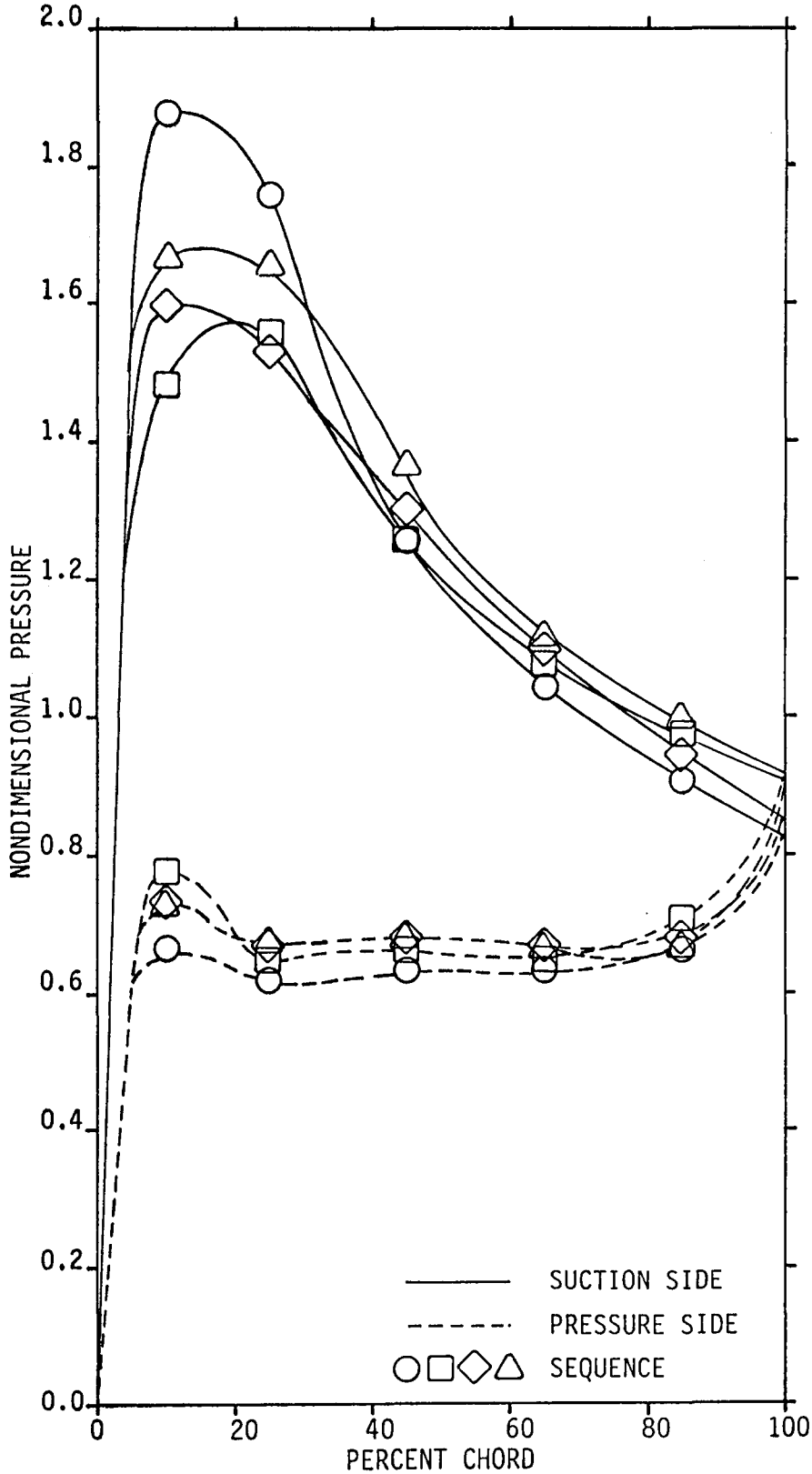

FIGURE 10a. SURGE BLADE PRESSURE DISTRIBUTION - 75% SPAN

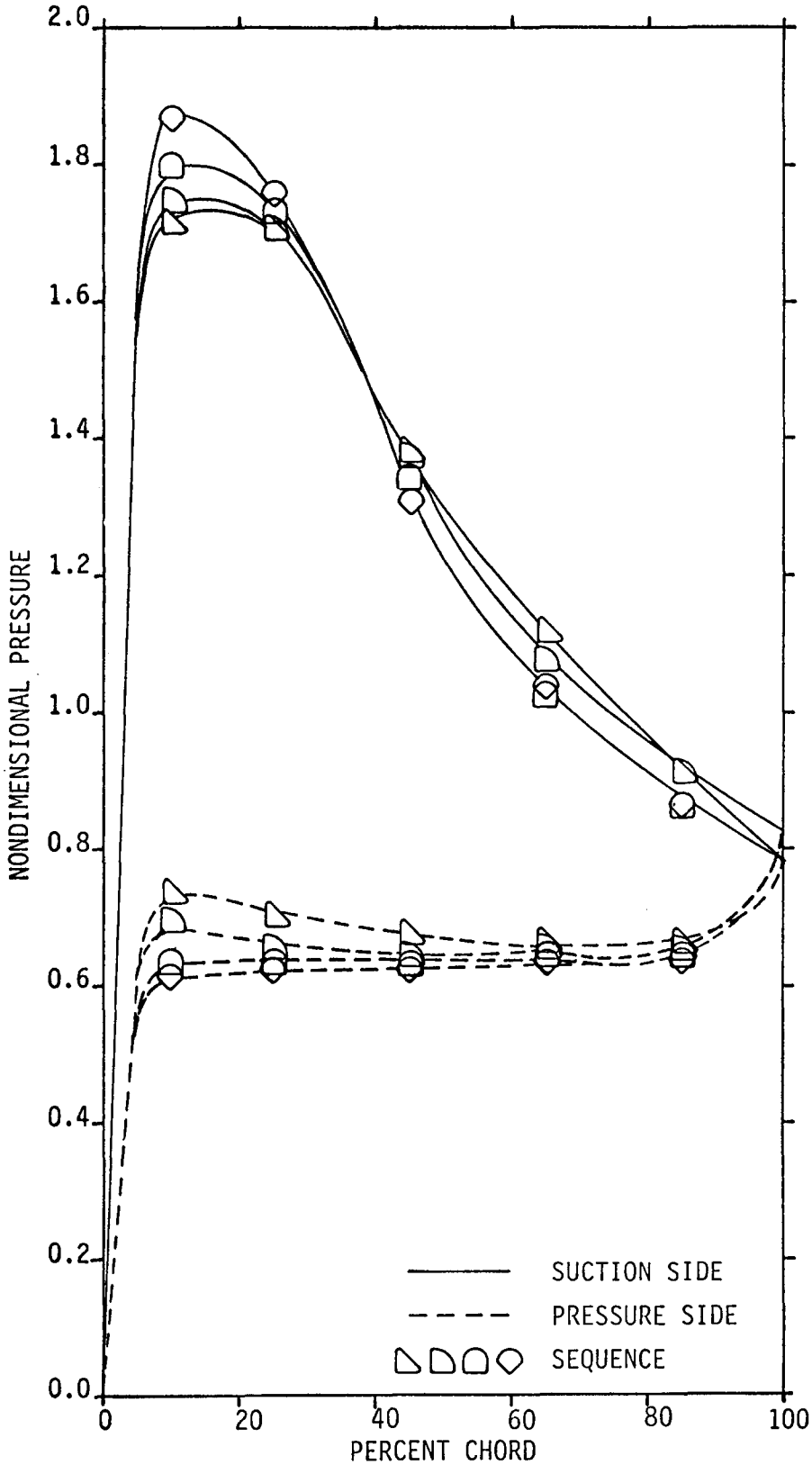

FIGURE 10b. SURGE BLADE PRESSURE DISTRIBUTION - 75% SPAN

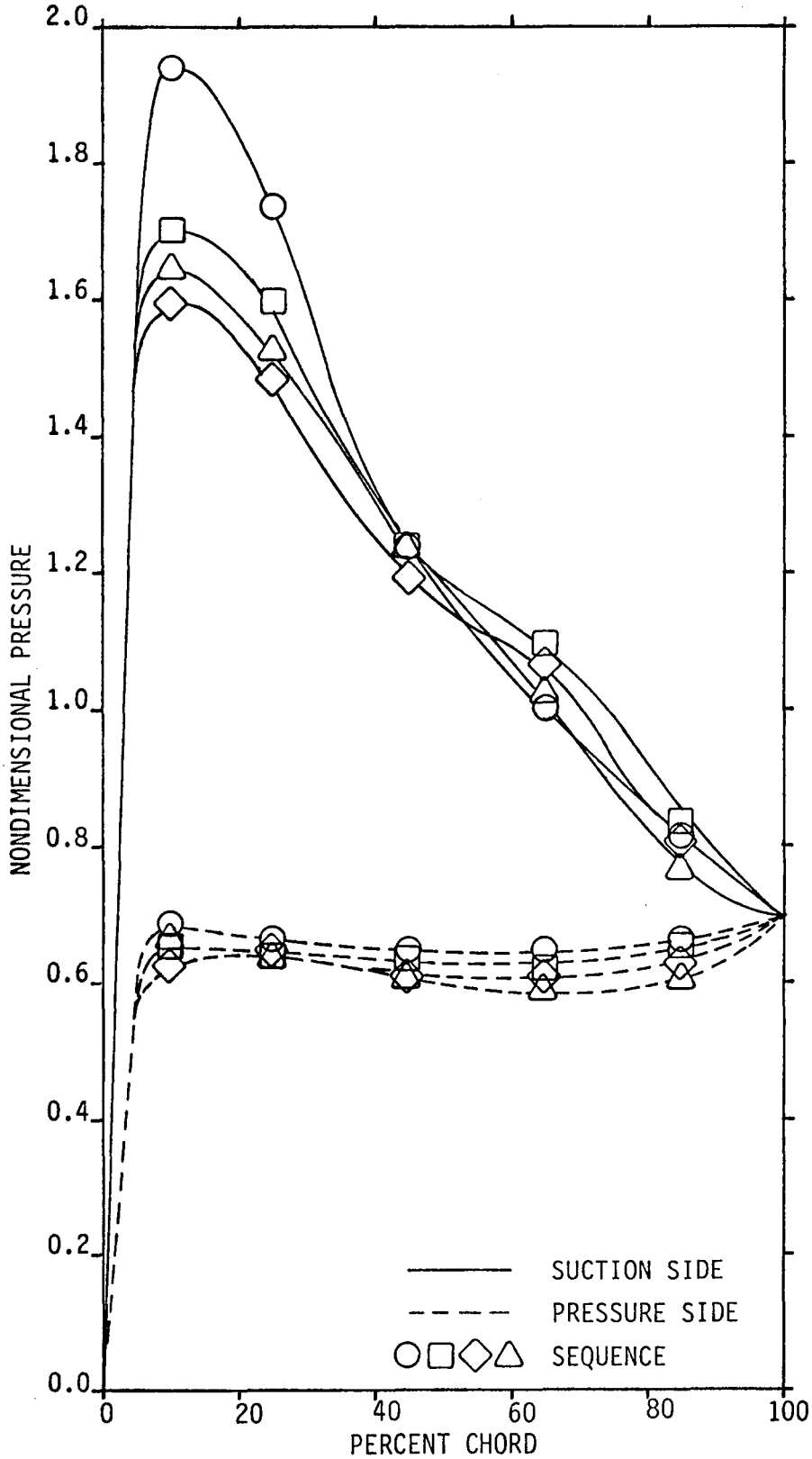

FIGURE 11a. SURGE BLADE PRESSURE DISTRIBUTION - 50% SPAN

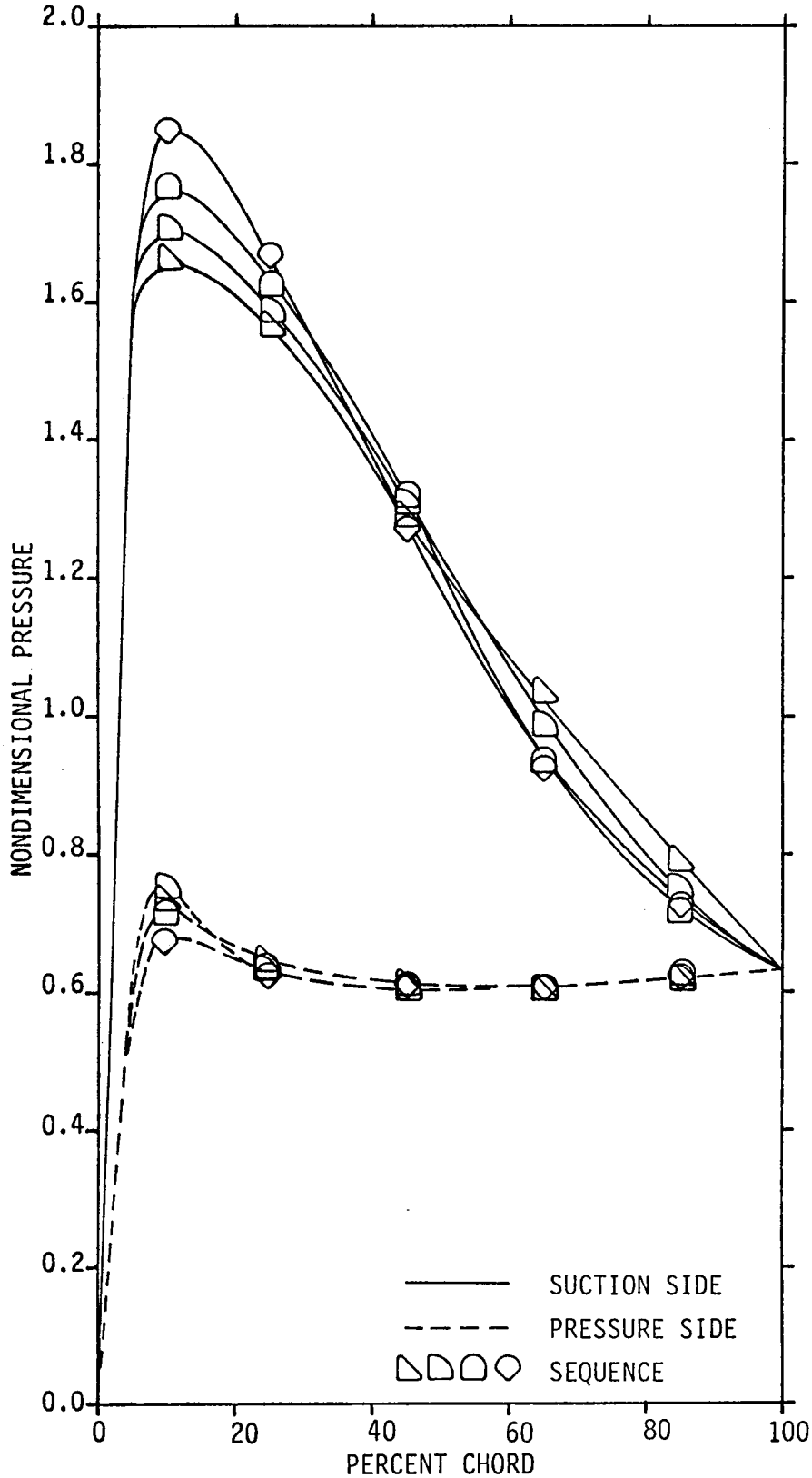

FIGURE 11b. SURGE BLADE PRESSURE DISTRIBUTION - 50% SPAN

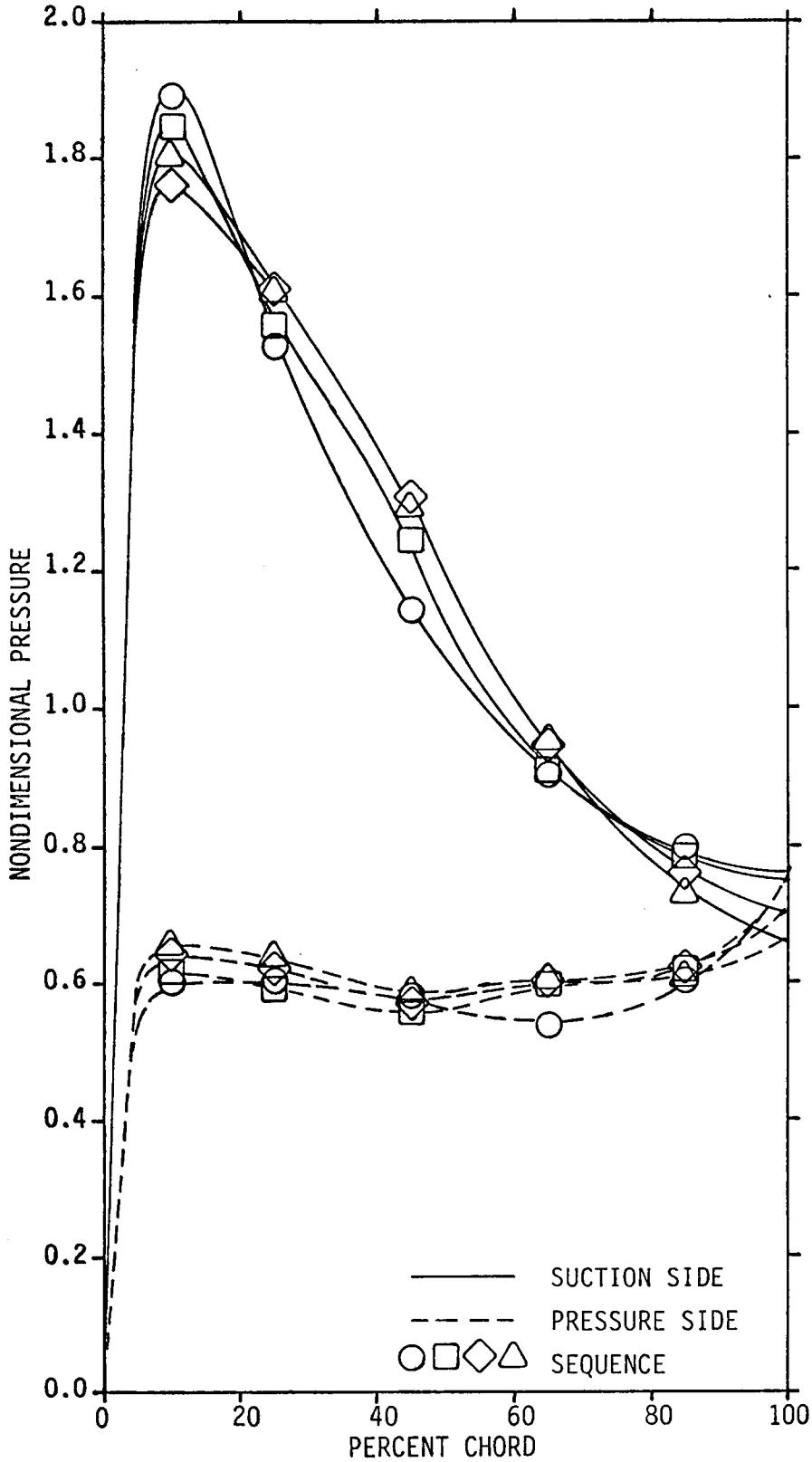

FIGURE 12a. SURGE BLADE PRESSURE DISTRIBUTION - 25% SPAN

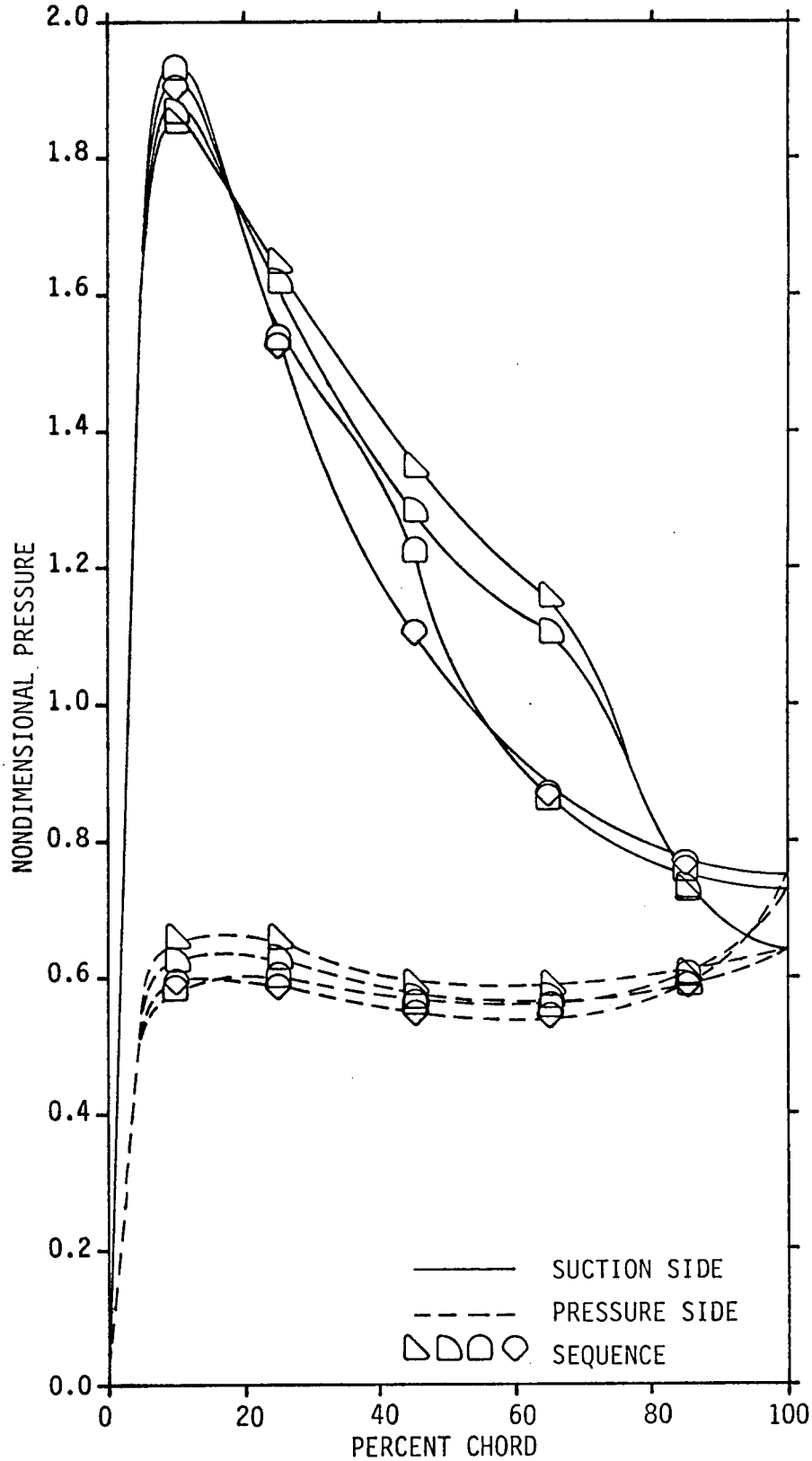

FIGURE 12b. SURGE BLADE PRESSURE DISTRIBUTION - 25% SPAN

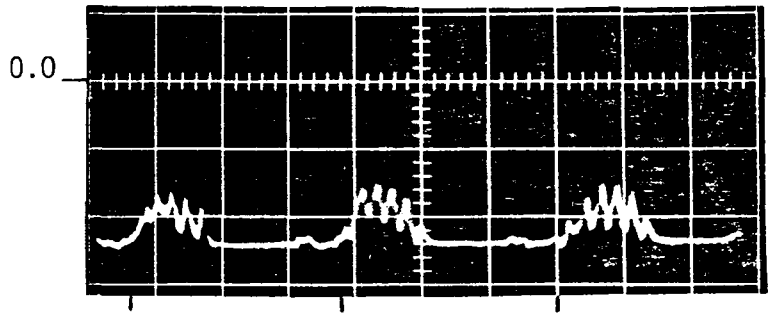

10% CHORD

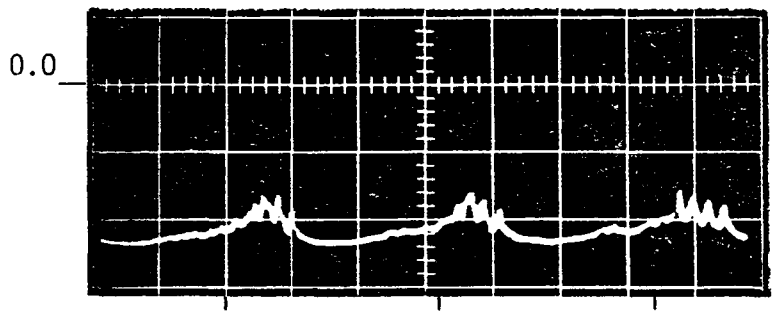

25% CHORD

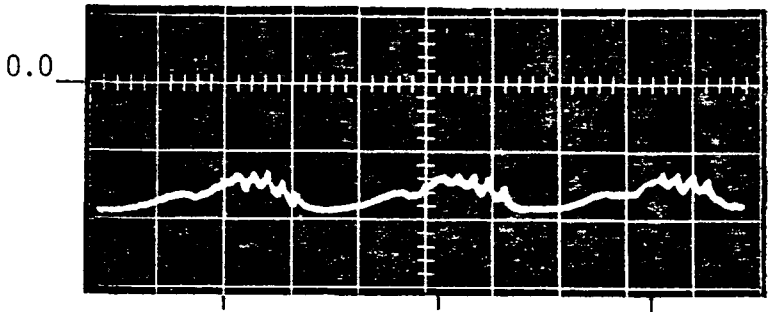

45% CHORD

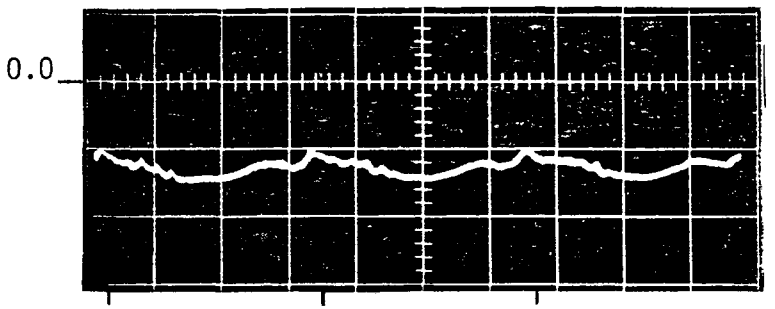

65% CHORD

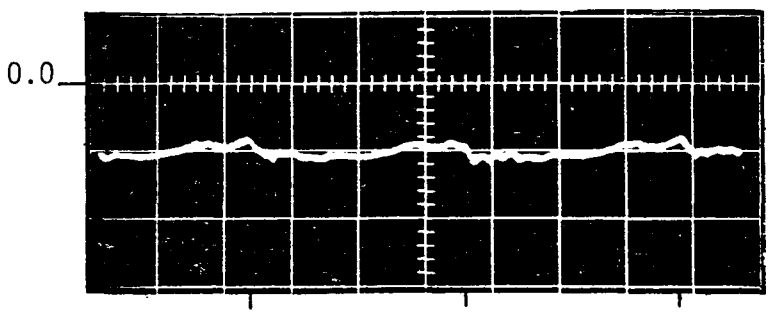

85% CHORD

TICK MARKS INDICATE TIME OF MINIMUM FLOW RATE

VERTICAL AXIS: PRESSURE, 1.49 kPa (6.0 in. H_2O) PER MAJOR GRATICULE

HORIZONTAL AXIS: TIME, 0.2 sec PER MAJOR GRATICULE

FIGURE 13a. SURGE BLADE PRESSURE TRACES - 75% SPAN SUCTION SIDE

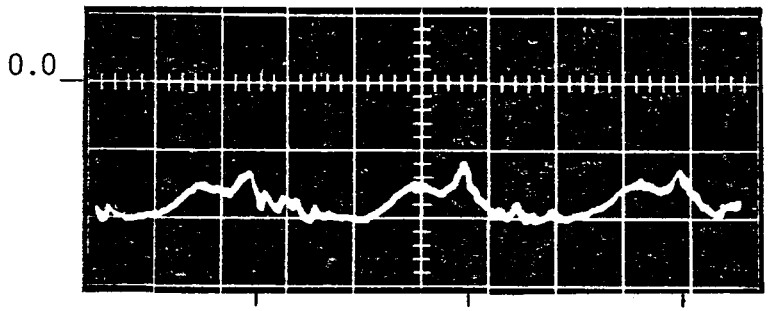

10% CHORD

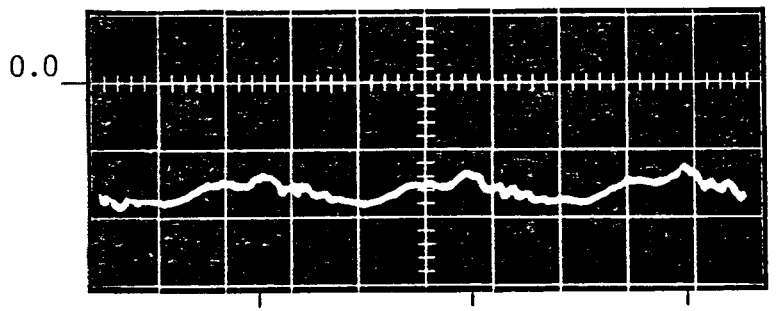

25% CHORD

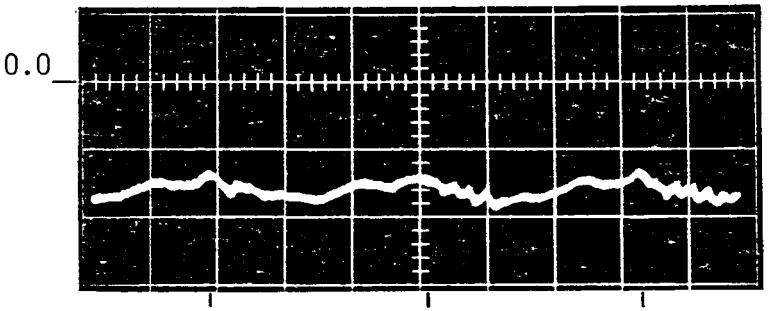

45% CHORD

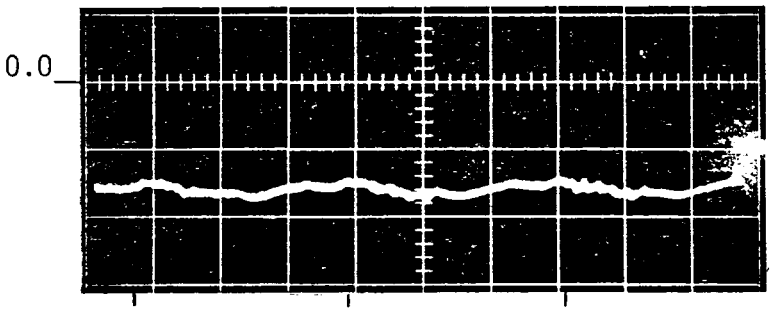

65% CHORD

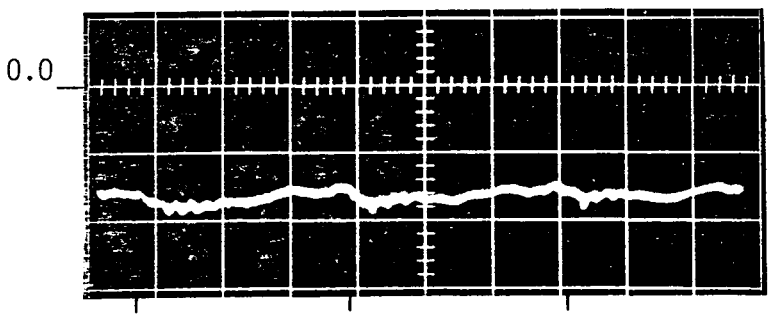

85% CHORD

TICK MARKS INDICATE TIME OF MINIMUM FLOW RATE

VERTICLE AXIS: PRESSURE, 0.60 kPa (2.4 in. H_2O) PER MAJOR GRATICULE

HORIZONTAL AXIS: TIME, 0.2 sec PER MAJOR GRATICULE

FIGURE 13b. SURGE BLADE PRESSURE TRACES - 75% SPAN PRESSURE SIDE

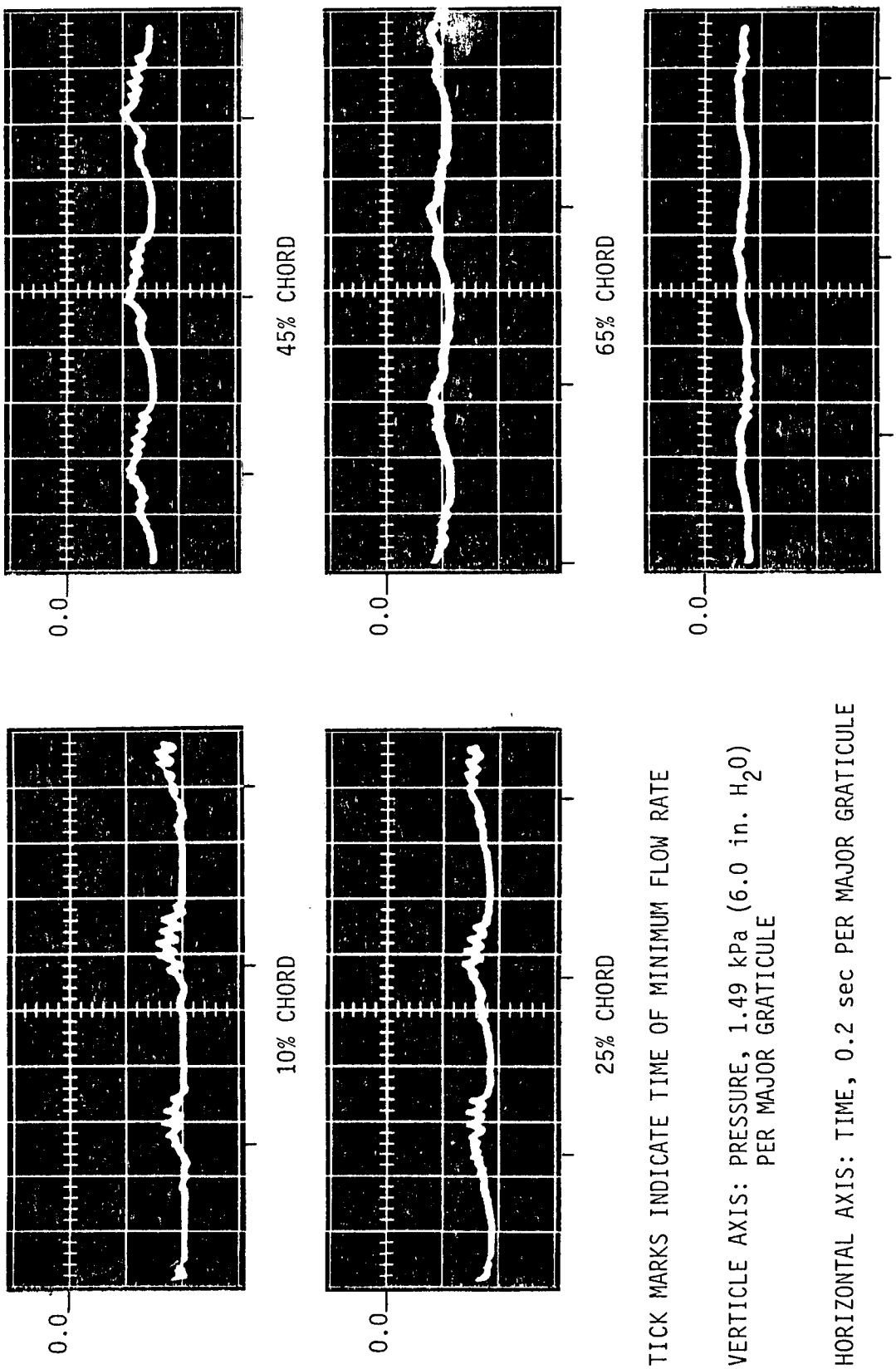

TICK MARKS INDICATE TIME OF MINIMUM FLOW RATE

VERTICLE AXIS: PRESSURE, 1.49 kPa (6.0 in. H_2O) PER MAJOR GRATICULE

HORIZONTAL AXIS: TIME, 0.2 sec PER MAJOR GRATICULE

FIGURE 14a. SURGE BLADE PRESSURE TRACES - 50% SPAN SUCTION SIDE

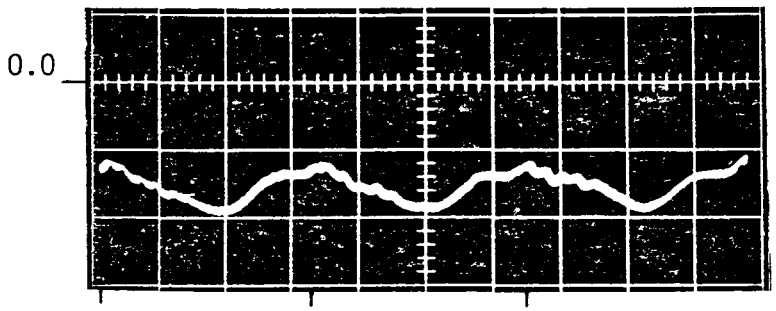

10% CHORD

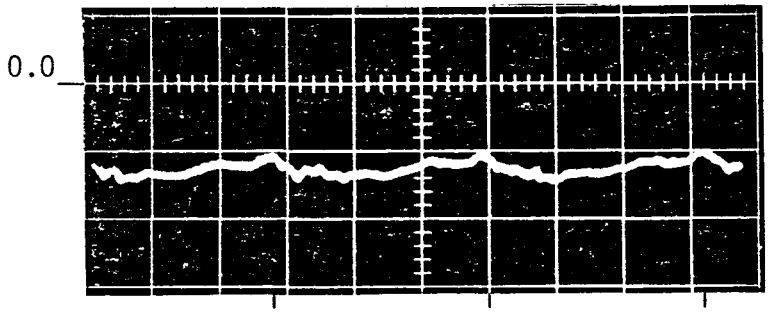

45% CHORD

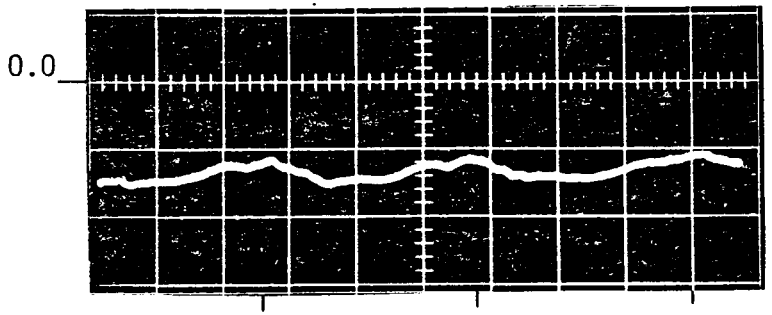

25% CHORD

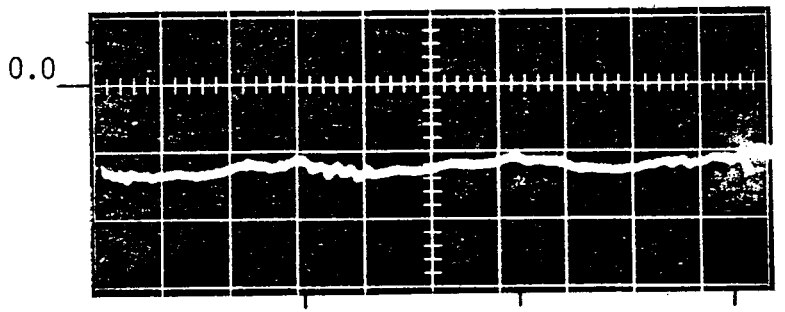

65% CHORD

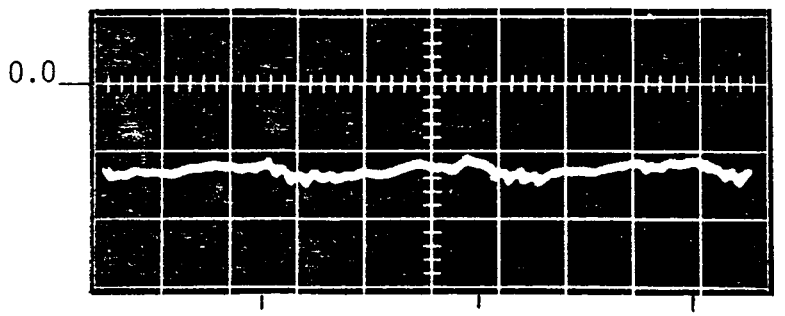

85% CHORD

TICK MARKS INDICATE TIME OF MINIMUM FLOW RATE

VERTICLE AXIS: PRESSURE, 0.60 kPa (2.4 in. H_2O) PER MAJOR GRATICULE

HORIZONTAL AXIS: TIME, 0.2 sec PER MAJOR GRATICULE

FIGURE 14b. SURGE BLADE PRESSURE TRACES - 50% SPAN PRESSURE SIDE

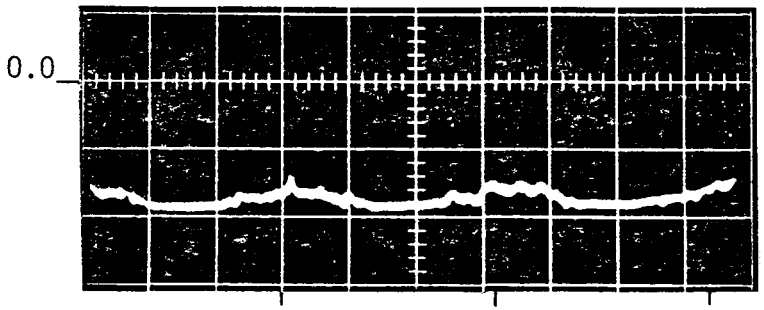

10% CHORD

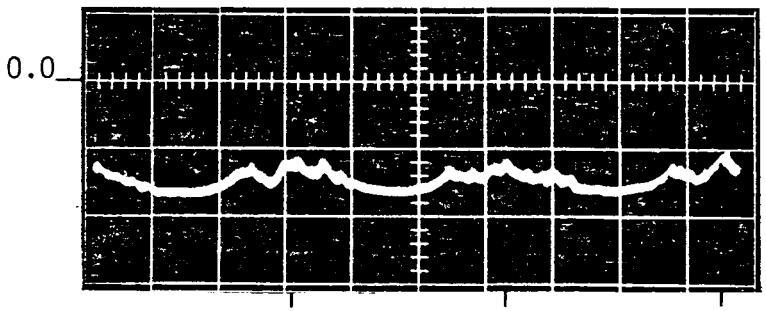

25% CHORD

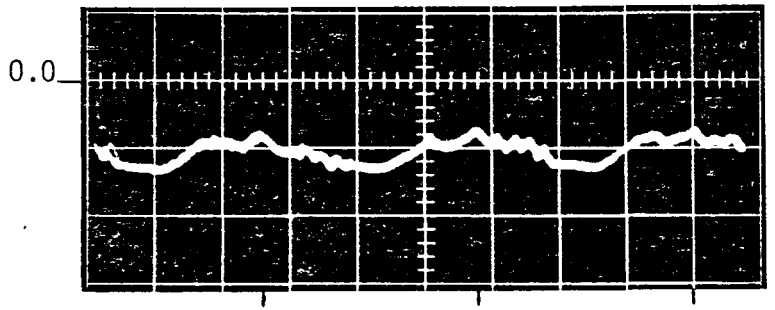

45% CHORD

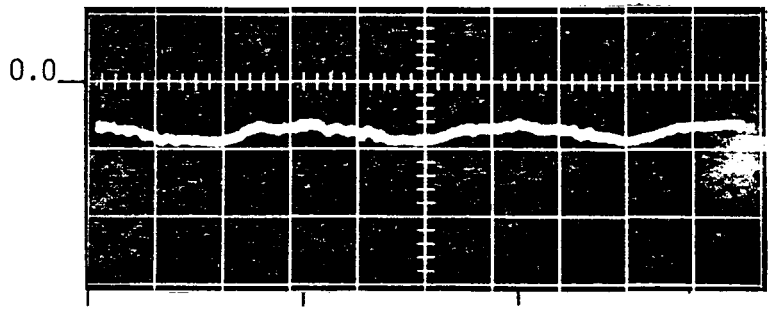

65% CHORD

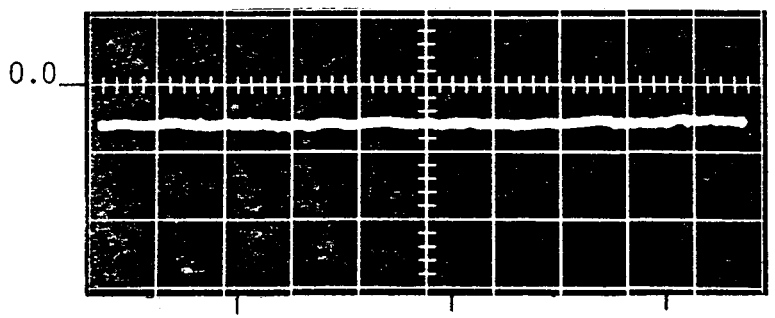

85% CHORD

TICK MARKS INDICATE TIME OF MINIMUM FLOW RATE

VERTICLE AXIS: PRESSURE, 1.49 kPa (6.0 in. H_2O) PER MAJOR GRATICULE

HORIZONTAL AXIS: TIME, 0.2 sec PER MAJOR GRATICULE

FIGURE 15a. SURGE BLADE PRESSURE TRACES - 25% SPAN SUCTION SIDE

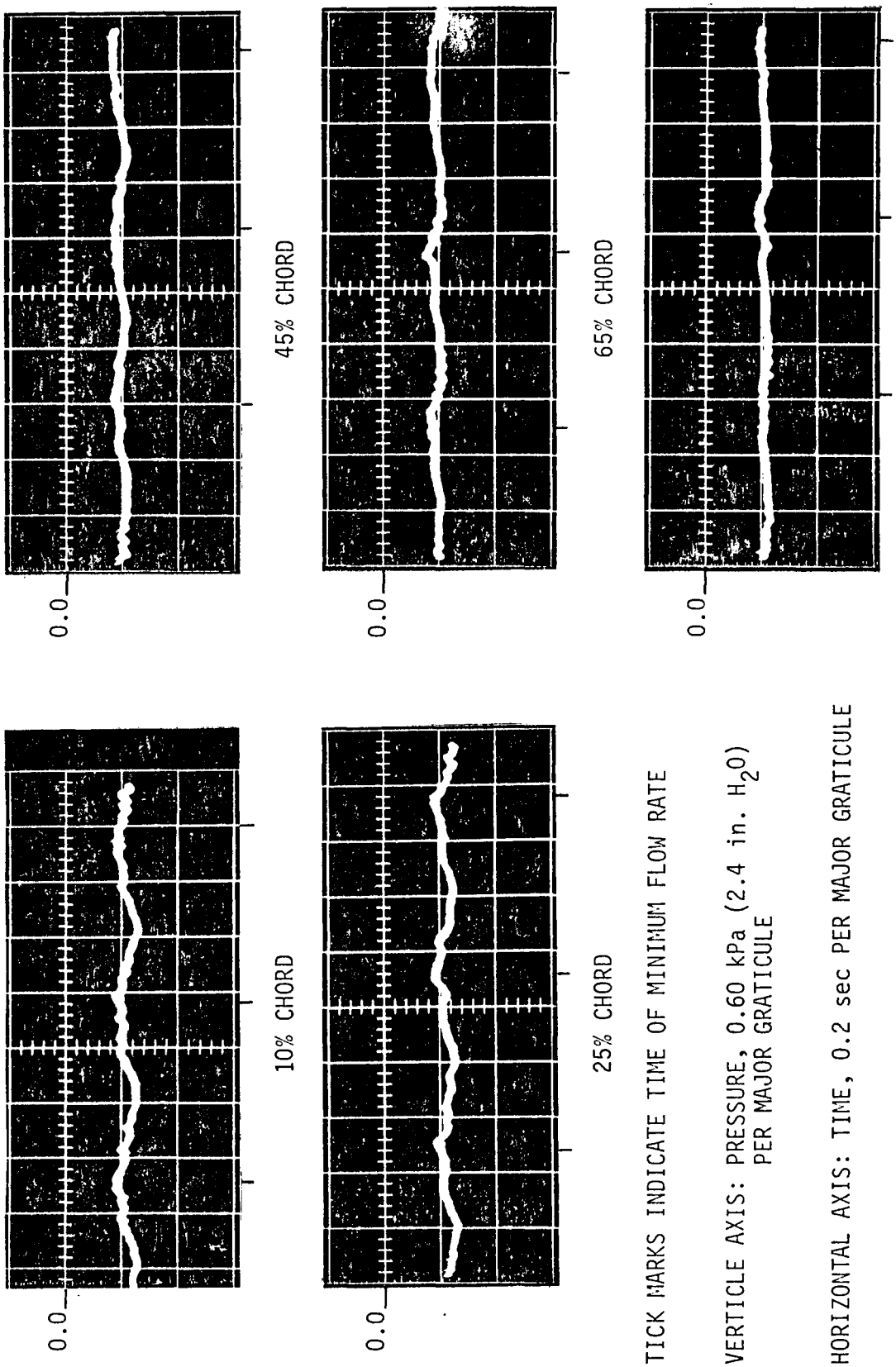

TICK MARKS INDICATE TIME OF MINIMUM FLOW RATE

VERTICLE AXIS: PRESSURE, 0.60 kPa (2.4 in. H_2O) PER MAJOR GRATICULE

HORIZONTAL AXIS: TIME, 0.2 sec PER MAJOR GRATICULE

FIGURE 15b. SURGE BLADE PRESSURE TRACES - 25% SPAN PRESSURE SIDE

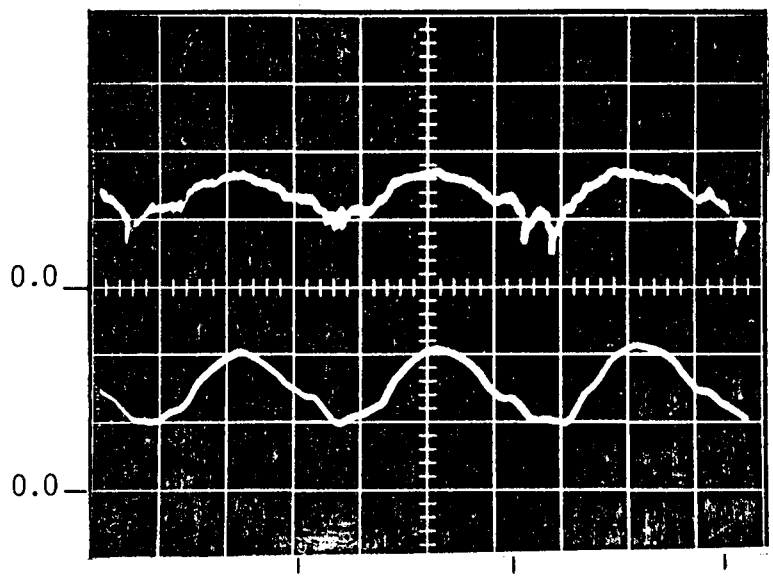

TICK MARKS INDICATE TIME OF MINIMUM FLOW RATE

VERTICLE AXIS:

TOP TRACE - TOTAL PRESSURE
0.30 kPa (1.2 in. H_2O)
PER MAJOR GRATICULE
ZERO AT FIFTH GRATICULE

BOTTOM TRACE - PITOT TUBE, DYNAMIC PRESSURE
0.10 kPa (0.40 in. H_2O)
PER MAJOR GRATICULE
ZERO AT SECOND GRATICULE

HORIZONTAL AXIS: TIME, 0.2 sec PER
MAJOR GRATICULE

FIGURE 16. SURGE BLADE TOTAL PRESSURE TRACE - 50% SPAN

The turning angle of the inlet guide vanes α_1, necessary for computing the absolute velocity downstream of the stators C_1, was obtained from experimental work done by Shultz [20] for the 50 percent span. The values of α_1 at the 75 and 25 percent span were determined by adjusting the 50 percent value by the angle of twist. This gives α_1 equal to 24, 22, and 20 degrees for the 75, 50, and 25 percent span positions respectively.

The steady-state nondimensional rotor blade pressure distributions obtained with the fixed plenum volume for the 75, 50, and 25 percent span positions are shown in Figs. 17, 18, and 19 respectively.

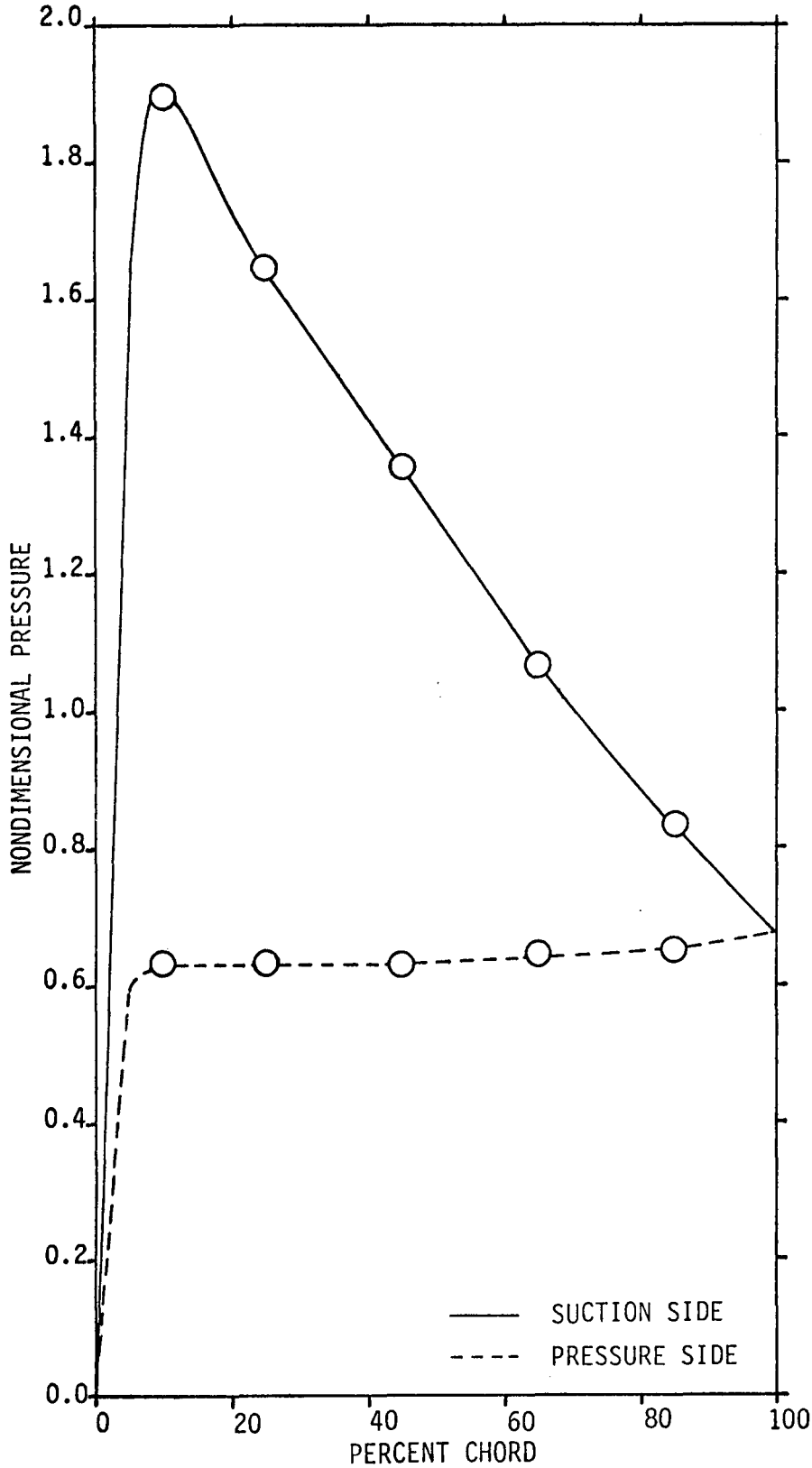

FIGURE 17. STEADY BLADE PRESSURE DISTRIBUTION - 75% SPAN

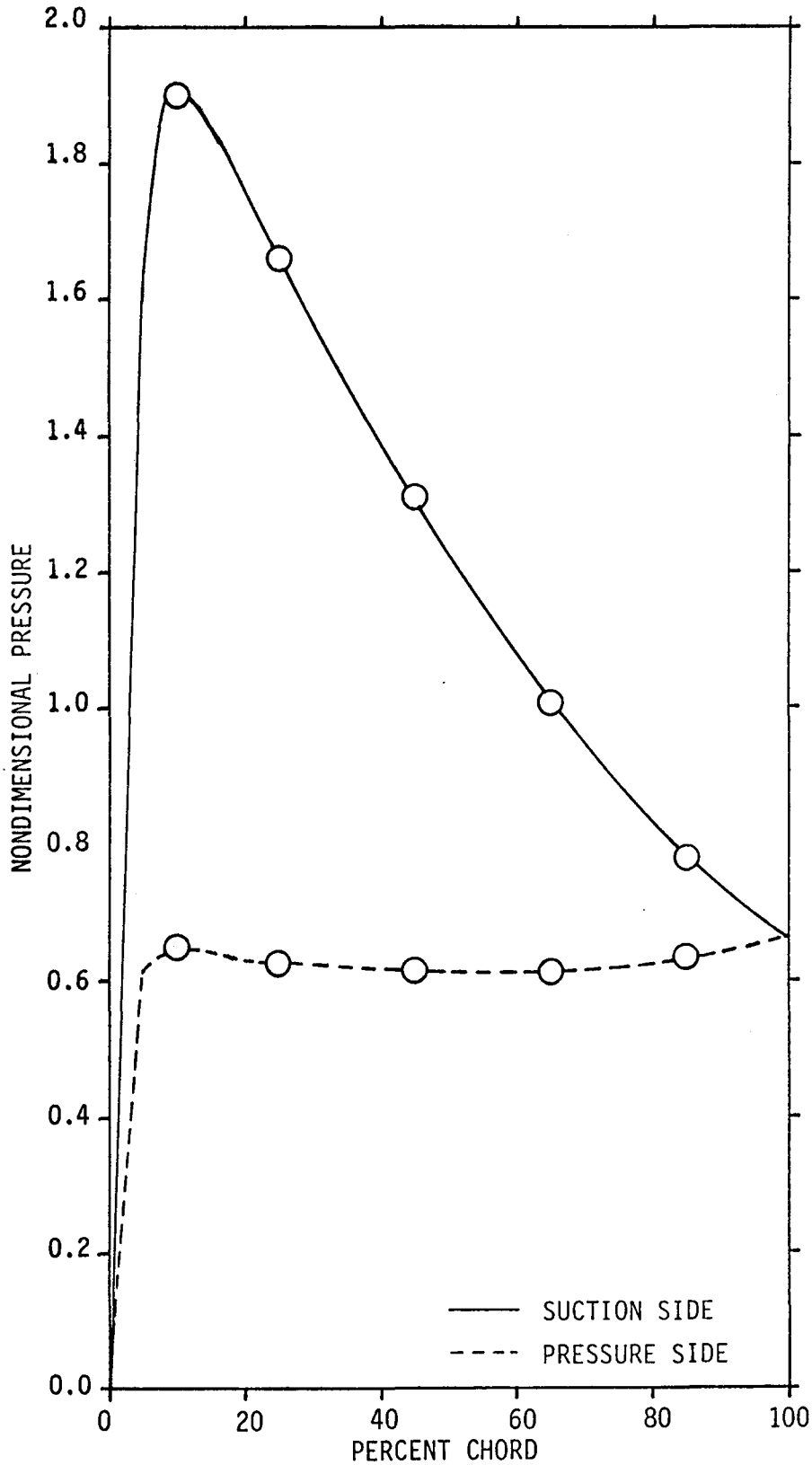

FIGURE 18. STEADY BLADE PRESSURE DISTRIBUTION - 50% SPAN

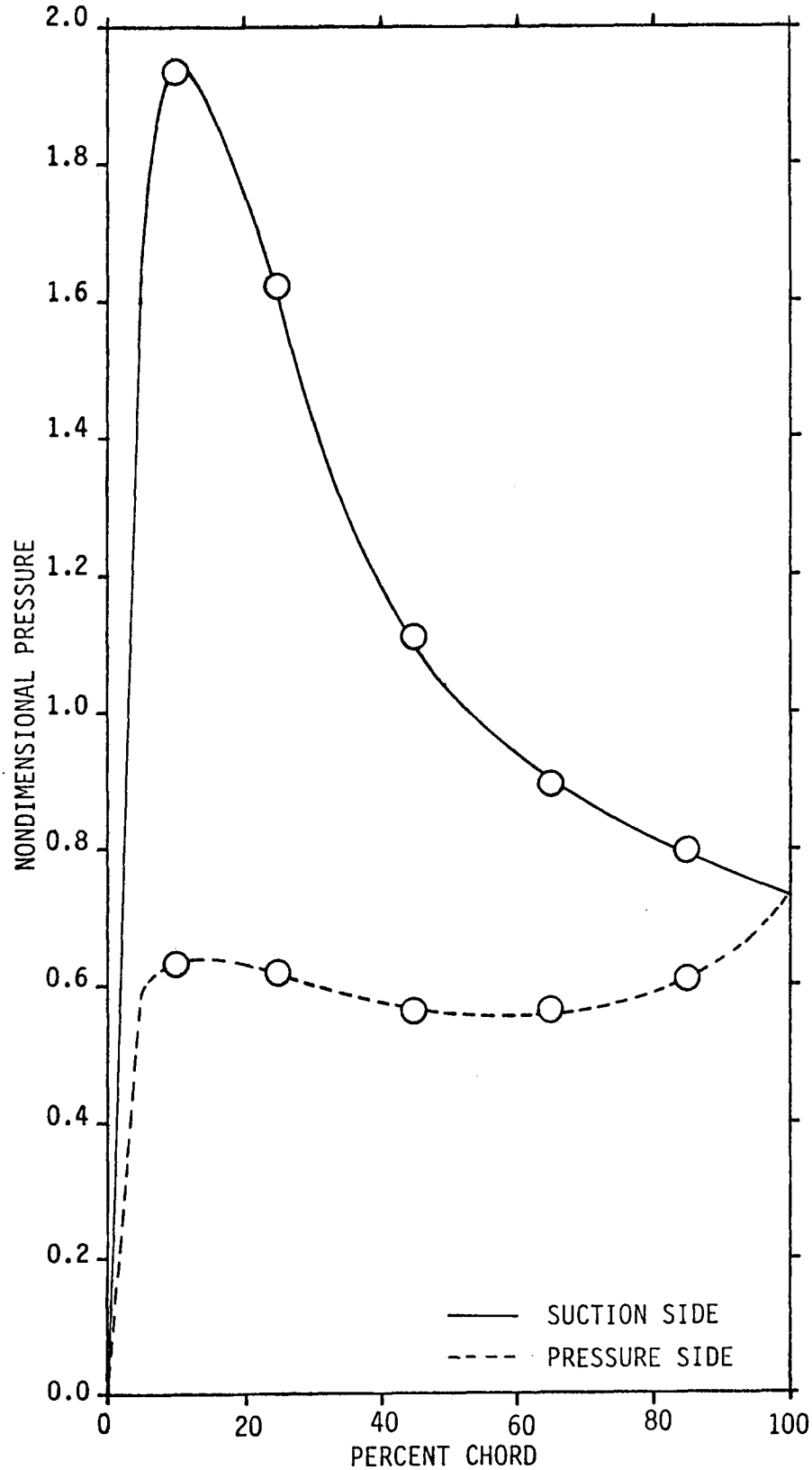

FIGURE 19. STEADY BLADE PRESSURE DISTRIBUTION - 25% SPAN

ANALYSIS

The purpose of this analysis is to investigate the stability of the compressor system tested in the experimental study of surge, using the measured compressor characteristic and the geometry of the compressor system. The mathematical model for surge presented by Greitzer [18] was applied to this system. A modification to the model was also made to include the effect of the flexible plenum top on the system stability.

Greitzer Model

In Greitzer's model, the compressor system is divided into five elements, the compressor, the plenum, the throttle, and the inlet and exit ducts. The compressor is modeled as an actuator disk, which affects a pressure rise in the inlet duct dependent on the associated mass flow rate. The throttle is assumed to be a nozzle which gives a pressure drop in the exit duct determined by the exit mass flow rate. The mass in each duct is lumped and inviscid. The volume of the plenum is fixed and compression of the fluid is assumed to take place isentropicly. A schematic of a compressor system is shown in Fig. 20. In this model all the kinetic energy is associated with the motion of fluid in the ducts. All the potential energy is in the form of compressed fluid in the plenum. This model assumes incompressible fluid in the ducts with a density equal to the ambient value. These assumptions limit the applicability of the model to low inlet Mach numbers and to pressure rises that are small relative to atmospheric pressure.

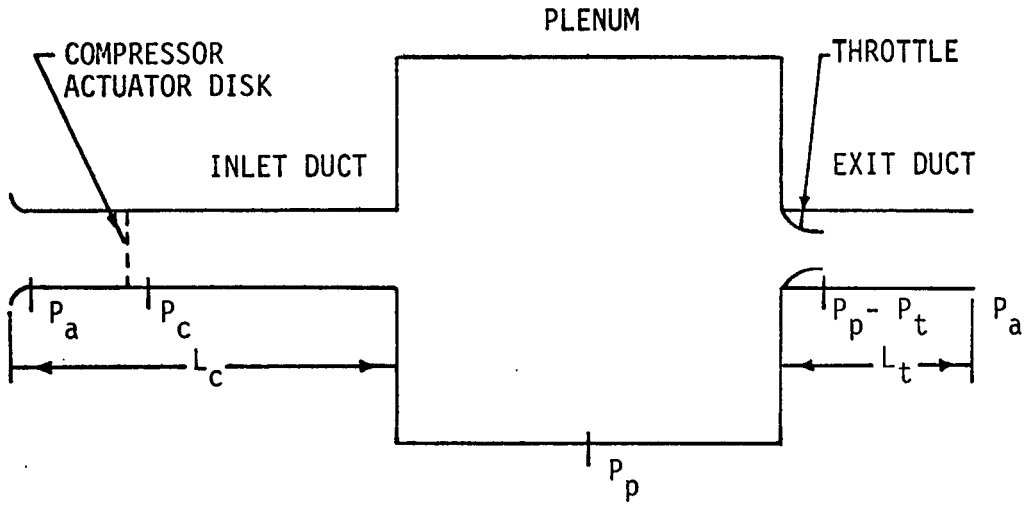

FIGURE 20. SCHEMATIC OF GREITZER MODEL

The acceleration of fluid in the compressor duct is due to a difference between the compressor pressure rise P_c and the plenum pressure relative to atmospheric pressure P_p. This relation is given by

$$\rho A_c L_c \frac{dC_c}{dt} = A_c(P_c - P_p) \quad , \tag{11}$$

where C is the fluid axial velocity, A is duct cross-sectional area, and L is duct length. The subscript c refers to the compressor, and ρ is ambient air density. This expression can be rewritten in terms of compressor mass flow rate $\dot{m}_c$ as

$$\frac{d\dot{m}_c}{dt} = \frac{A_c}{L_c}(P_c - P_p) \quad . \tag{12}$$

With P_t as the pressure drop across the throttle, a similar expression for the acceleration of mass flow rate in the throttle duct is given by

$$\frac{d\dot{m}_t}{dt} = \frac{A_t}{L_t}(P_p - P_t) \quad , \tag{13}$$

where the subscript t indicates the duct associated with the throttle.

Any difference in the mass flow rates through the inlet or exit ducts will cause a change in the fluid density in the plenum. This relation can be expressed as

$$V_p \frac{d\rho_p}{dt} = (\dot{m}_c - \dot{m}_t) \quad , \tag{14}$$

where V is volume, and the subscript p refers to the plenum. The change in fluid density with respect to time for an isentropic compression is given by

$$\frac{d\rho_p}{dt} = \frac{\rho_p}{\gamma P_p} \frac{dP_p}{dt} \quad , \tag{15}$$

where γ is the specific heat ratio of the fluid. Experiments by Greitzer [19] have shown the isentropic compression assumption to be reasonable. Substituting Eq. 15 into Eq. 14 and rearranging yields

$$\frac{dP_p}{dt} = \frac{\gamma P_p}{\rho V_p}(\dot{m}_c - \dot{m}_t) \quad . \tag{16}$$

The pressure rise across the compressor is a function of the mass flow rate and is obtained from the compressor characteristic. Since the response of the compressor to changes in mass flow rate is not instantaneous, this time lag is taken into account in the model with a time constant. The relation is expressed by

$$\frac{dP_c}{dt} = \frac{1}{\tau}(P_{cs} - P_c) \quad , \tag{17}$$

where τ is the time constant and P_{cs} is the pressure rise across the compressor given by the steady-state compressor map. The time constant is assumed proportional to the time for some number of rotor revolutions N through the relation

$$\tau = 2\pi NR/U \quad , \tag{18}$$

where R is the blade tip radius and U the rotor tip speed.

The pressure drop across the throttle is proportional to the square of the velocity through it as given by

$$P_t = \tfrac{1}{2} K\rho C_t^2 \quad , \tag{19}$$

where K is determined for the specific throttle used. For incompressible inviscid flow, K is 1. Equation 19 is written in terms of throttle mass flow rate as

$$P_t = \frac{K\dot{m}_t^2}{2\rho A_t^2} \quad . \tag{20}$$

Equations 12, 13, 16, 17, and 20 and the steady-state compressor characteristic govern the fluid dynamics of the compressor system. These equations can be nondimensionalized by dividing pressure by $\frac{1}{2}\rho U^2$, mass flow rate by $\rho U A_c$ and time by the Helmholtz resonator frequency of the system. The expression for the resonator frequency ω is

$$\omega = a\sqrt{A_c/(V_p L_c)} \tag{21}$$

where a is the speed of sound in air at ambient conditions. With (~) designating nondimensional variables, the resulting equations are:

$$\frac{d\tilde{\dot{m}}_c}{d\tilde{t}} = B(\tilde{P}_c - \tilde{P}_p) \tag{22}$$

$$\frac{d\tilde{\dot{m}}_t}{d\tilde{t}} = (B/G)(\tilde{P}_p - \tilde{P}_t) \tag{23}$$

$$\frac{d\tilde{P}_p}{d\tilde{t}} = (1/B)(\tilde{\dot{m}}_c - \tilde{\dot{m}}_t) \tag{24}$$

$$\frac{d\tilde{P}_c}{d\tilde{t}} = (1/\tilde{\tau})(\tilde{P}_{cs} - \tilde{P}_c) \tag{25}$$

$$\tilde{P}_t = KA^2\tilde{\dot{m}}_t^2 \tag{26}$$

$$\tilde{P}_c = f(\tilde{\dot{m}}_c) \quad . \tag{27}$$

The nondimensional system parameters involved, A, B, and G, are:

$$A = \frac{A_t}{A_c} \tag{28}$$

$$B = \frac{U}{2a}\sqrt{V_p/(A_c L_c)} \tag{29}$$

$$G = \frac{L_t A_c}{L_c A_t} \tag{30}$$

$$\tilde{\tau} = 2\pi NR\omega/U \quad . \tag{31}$$

Using the expression for B

$$\tilde{\tau} = (\pi R/L_c)(N/B) \quad . \tag{32}$$

Flexible Plenum Model

The compressor system on which the surge experiment was done has a flexible top described in the equipment section of the experiment. To obtain an estimate of what effect this arrangement has on the system stability a simplified model was derived for the plenum and applied to Greitzer's model.

The model of the plenum is composed of a movable piston inserted in a container that has constant cross section and is closed at one end. The piston has an associated mass that is supported by a spring. A schematic of the system is shown in Fig. 21.

The governing equations are the same as those used in Greitzer's model except for Eq. 16 and its nondimensional form, Eq. 24. The change in mass stored in the plenum is no longer a function of plenum fluid density alone. The relation for stored mass is now

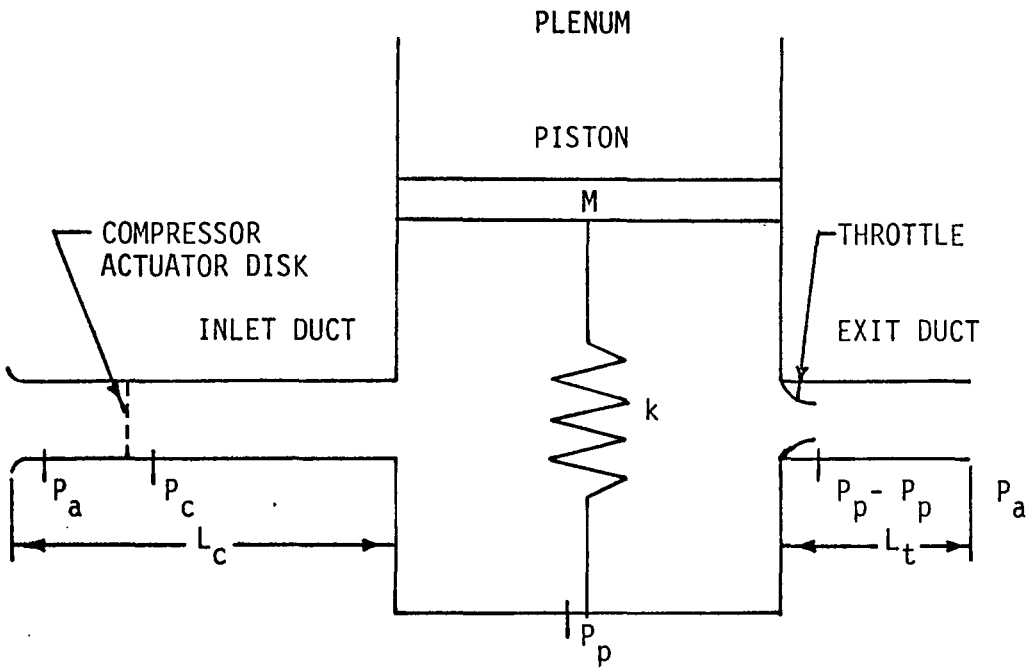

FIGURE 21. SCHEMATIC OF FLEXIBLE PLENUM MODEL

$$\frac{dm_p}{dt} = \frac{d}{dt}(\rho_p V_p) \tag{33}$$

$$\frac{dm_p}{dt} = \frac{d\rho_p}{dt} V_p + \rho_p \frac{dV_p}{dt} \quad . \tag{34}$$

Equation 15 gives the relation for the first term on the righthand side of Eq. 34. The derivative of the plenum volume is dependent on the displacement of the piston. The expression for the piston displacement x is given by

$$\frac{Md^2x}{dt^2} \pm kx^n = P_p A_p - Mg \quad , \tag{35}$$

where M is the mass of the piston, k is the spring constant, n is an integer exponent, and A_p is the piston area. For a linear spring, n is 1. The sign of the kx^n term is the same as the sign of x. Rearranging and integrating Eq. 35 yields

$$\frac{dx}{dt} = \int_0^t (P_p A_p \mp kx^n - Mg)/M \, dt \quad . \tag{36}$$

The change in volume with respect to time is then

$$\frac{dV_p}{dt} = A_p \frac{dx}{dt} \quad . \tag{37}$$

The plenum volume V_p is given by

$$V_p = \bar{V}_p + \int_0^t A_p \frac{dx}{dt}\, dt \quad , \tag{38}$$

where $\bar{V}_p$ is fixed plenum volume. Substituting the relations given in Eqs. 15 and 37 into Eq. 34 yields

$$\frac{dm_p}{dt} = \frac{\rho_p V_p}{\gamma P_p} \frac{dP_p}{dt} + \rho_p A_p \frac{dx}{dt} \quad . \tag{39}$$

Rearranging Eq. 39 to get an explicit form for the change in plenum pressure with respect to time gives

$$\frac{dP_p}{dt} = \frac{\gamma P_p}{\rho_p V_p} \frac{dm_p}{dt} - \frac{\gamma P_p A_p}{V_p} \frac{dx}{dt} \quad . \tag{40}$$

Equations 22, 23, 25, 26, 27, 35, and 40 govern the fluid dynamics of this compressor system. Equations 35 and 40 are nondimensionalized by multiplying the piston displacement by $A_p/\bar{V}_p$. The other parameters are nondimensionalized in the same manner as before. The nondimensional forms of Eqs. 35 and 40 are:

$$\frac{d^2\tilde{x}}{d\tilde{t}^2} = E\tilde{P}_p + F\tilde{x}^n - J \tag{41}$$

$$\frac{d\tilde{P}_p}{d\tilde{t}} = (H/B)(\dot{\tilde{m}}_c - \dot{\tilde{m}}_t) - \gamma H^2 \tilde{P}_p \frac{d\tilde{x}}{d\tilde{t}} \tag{42}$$

where the new nondimensional parameters E, F, H, and J are:

$$E = \frac{\frac{1}{2}\rho U^2 A_p^2}{M\omega^2 \bar{V}_p} \tag{43}$$

$$F = \frac{k}{M\omega^2} \frac{\bar{V}_p^{n-1}}{A_p^{n-1}} \tag{44}$$

$$H = \sqrt{\bar{V}_p / V_p} \quad . \tag{45}$$

$$J = \frac{g}{\omega^2} \frac{A_p}{\bar{V}_p} \tag{46}$$

It should be noted that H is a variable dependent on the instantaneous plenum volume.

Numerical Analysis

The IBM Continuous System Modeling Program (CSMP), program number 360A-CS-16Xm, was used to numerically model the operation of the system. The program uses fourth-order Runge-Kutta integration. Differentiation is available but was avoided since it introduces more error than integration.

Greitzer [18] indicates that the time constant is about equal to the value given by 2 rotor revolutions and has little effect on the stability of the system, so the value is not critical but represents

the order of magnitude of the response time of the compressor. The value of N for determining the time constant was varied between 0.1 and 3.0 to investigate the effect it has on the system stability.

The compressor characteristic was available to the program in the form of an arbitrary function generator subroutine. This program interpolates linearly between given points on the curve. A starting point for the program was chosen so that the throttle setting, mass flow rate and plenum pressure coincided with the point on the compressor map that was of interest.

A block diagram for solution of the set of governing equations for Greitzer's model is given in Fig. 22.

In choosing values for the flexible plenum parameters, the volume was assumed to change a fraction I of the fixed plenum volume during charging of the plenum from zero to maximum pressure. The expression for determining the spring constant is

$$K = (P_{pmax}A_p - Mg)A_p^n/(I\bar{V}_p)^n \qquad (47)$$

where P_{pmax} is the maximum plenum pressure. The value of the piston area used was determined by

$$A_p = (\bar{V}_p)^{2/3} \quad . \qquad (48)$$

The value of I was varied between 0.05 and 0.20 to determine its effect on the form of the surge cycle, since it could not be measured

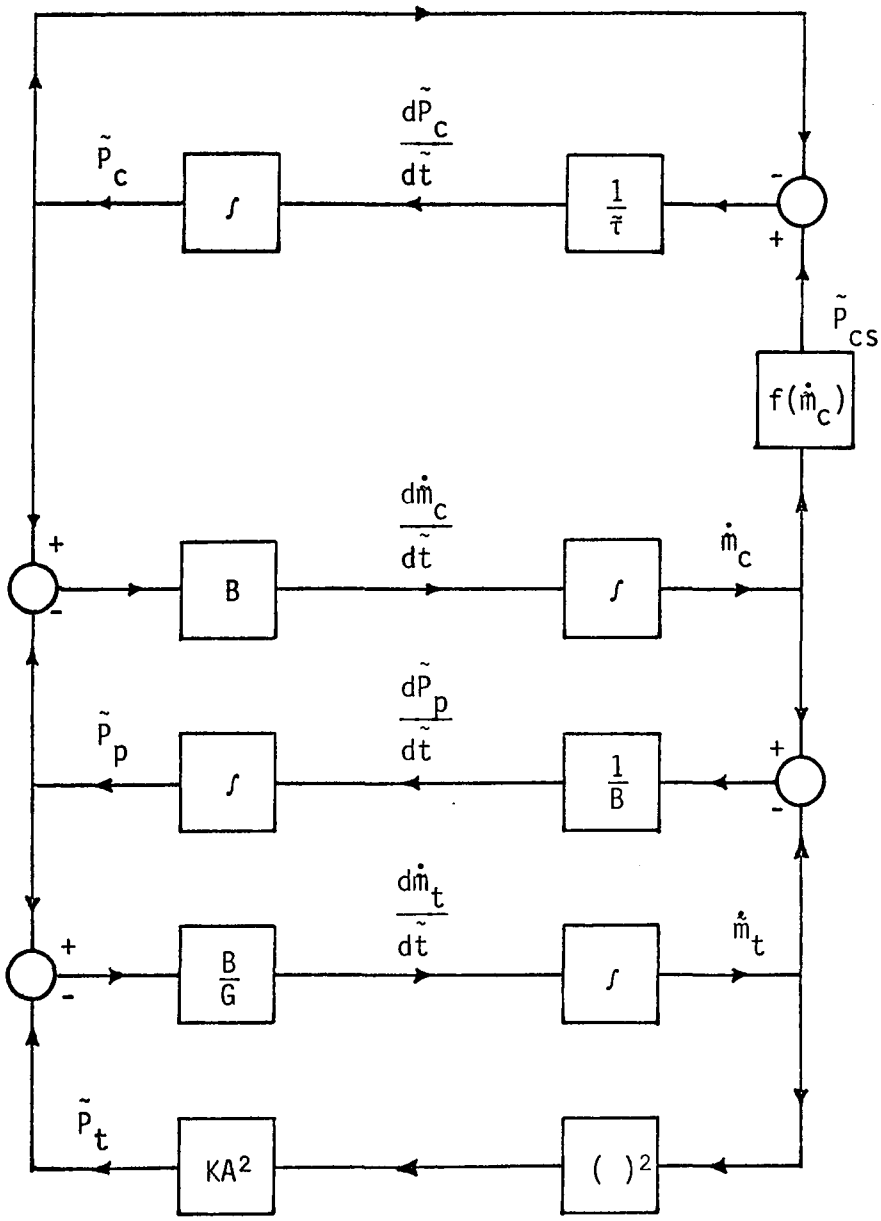

FIGURE 22. BLOCK DIAGRAM OF GREITZER MODEL

accurately from the actual equipment. The value of n was varied between one and seven to investigate the effects of linear and non-linear springs.

A block diagram for solution of the set of equations governing the compressor system with a flexible plenum top is given in Fig. 23.

Analytical Results

The analytical study of the fixed plenum volume compressor system shows that the compressor will surge for large values of the B parameter by being forced to operate on the positively-sloped portion of the compressor characteristic. The throttle position used for this analysis corresponds to position 3 in the experimental system.

The minimum value of B at which surge occurs varies with the time constant used. At a very small time constant, approximating instantaneous response of the compressor to changes in mass flow, the inception of surge occurs between B equal to 1.2 and 1.3. The minimum value of B at which surge occurs for a time constant corresponding to one rotor revolution is between 1.4 and 1.5, for two rotor revolutions it is between 1.6 and 1.7, and for three rotor revolutions it is between 1.7 and 1.8. The surge is very mild, corresponding to limit cycle surge, for the minimum value of B at which an instability occurs. As B is increased above the limiting value the surge gradually becomes stronger.

The magnitude of the fluctuations of mass flow rate and plenum pressure for the time constants corresponding to 0.1, 1, 2, and 3

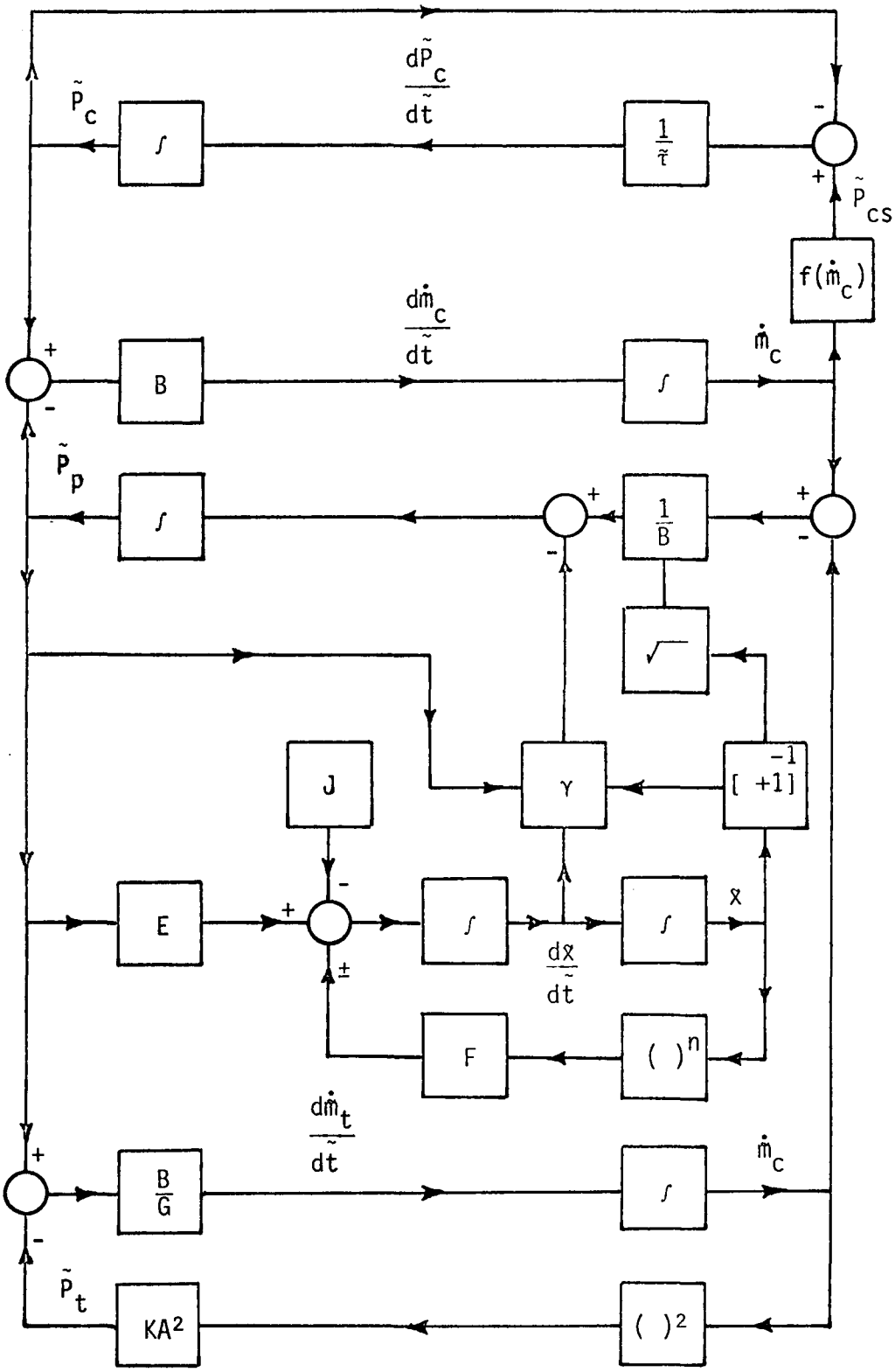

FIGURE 23. BLOCK DIAGRAM OF FLEXIBLE PLENUM MODEL

rotor revolutions are given in Tables 2, 3, 4, and 5 respectively for the values of B evaluated. A steady-state surge cycle for B equal to 1.8 and a time constant corresponding to one rotor revolution is shown on the steady-state compressor map in Fig. 24.

The analysis of the flexible plenum model showed little if any fluctuation in the mass flow rate or plenum pressure for the values of n investigated. These results indicate that the spring mass systems used are not good approximations of the effect of the highly nonlinear rubber diaphram and mass system used in the experimental system.

Table 2. Analytical Surge Limits - N of 0.1

B	$\tilde{P}_{pmax}$	$\tilde{P}_{pmin}$	$\dot{\tilde{m}}_{cmax}$	$\dot{\tilde{m}}_{cmin}$
1.3	0.314	0.303	0.272	0.260
1.4	0.325	0.294	0.286	0.246
1.5	0.369	0.220	0.353	0.155
1.6	0.390	0.190	0.411	0.110
1.7	0.387	0.192	0.415	0.106
1.8	0.383	0.196	0.418	0.104
1.9	0.380	0.199	0.421	0.101
2.0	0.377	0.202	0.423	0.100

Table 3. Analytical Surge Limits - N of 1.0

B	$\tilde{P}_{pmax}$	$\tilde{P}_{pmin}$	$\dot{\tilde{m}}_{cmax}$	$\dot{\tilde{m}}_{cmin}$
1.5	0.313	0.304	0.271	0.260
1.6	0.323	0.295	0.286	0.245
1.7	0.363	0.227	0.353	0.157
1.8	0.380	0.201	0.417	0.109
1.9	0.376	0.205	0.420	0.104
2.0	0.372	0.208	0.423	0.102

Table 4. Analytical Surge Limits - N of 2.0

B	$\tilde{P}_{pmax}$	$\tilde{P}_{pmin}$	$\dot{\tilde{m}}_{cmax}$	$\dot{\tilde{m}}_{cmin}$
1.7	0.311	0.307	0.269	0.263
1.8	0.319	0.300	0.281	0.252
1.9	0.330	0.289	0.301	0.235
2.0	0.372	0.201	0.418	0.111

Table 5. Analytical Surge Limits - N of 3.0

B	$\tilde{P}_{pmax}$	$\tilde{P}_{pmin}$	$\dot{\tilde{m}}_{cmax}$	$\dot{\tilde{m}}_{cmin}$
1.8	0.3088	0.3087	0.2661	0.2656
1.9	0.3100	0.3074	0.2678	0.2638
2.0	0.3158	0.3019	0.2771	0.2536

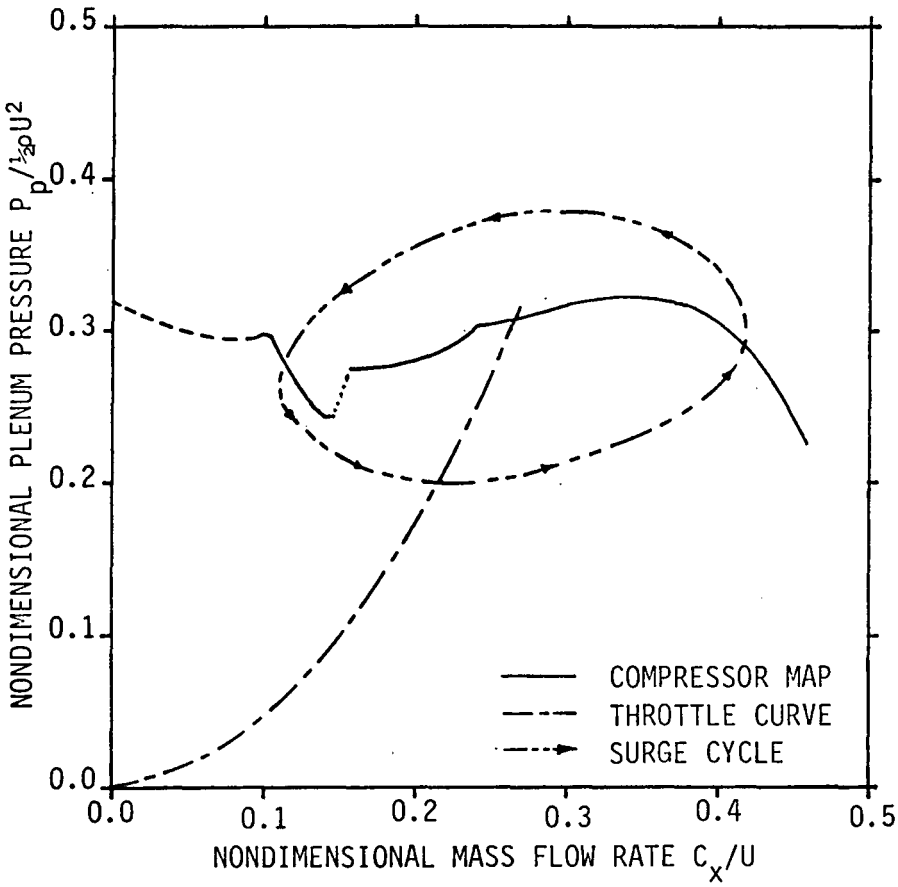

FIGURE 24. ANALYTICAL SURGE CYCLE - B OF 1.8, N OF 1

DISCUSSION OF RESULTS

The steady-state compressor characteristic indicates that the stall that a compressor operates under can be of more than one form and is a repeatable function of mass flow rate. This phenomenon is demonstrated by detection of rotating stall and full-rotor part-span stall occuring over two different portions of the stalled region of the compressor map.

The inlet velocity distribution determined during the surge cycle shows a noticeable retardation of the flow near the outside radius of the inlet annulus. This reduced flow is a possible indication of separation or stall near the rotor tip. The hot wire traces show rotating stall occuring over a range of low mass flow rates in the cycle.

The experimentally-determined surge cycle shows that the plenum pressure drops at low flow and remains low until its recovery begins at a high mass flow rate. The spacing of the data points indicates that stall occurs rapidly, and the recovery rate is slower.

The rotor blade pressure distributions measured during surge indicate that stall occurs very rapidly near the point of minimum mass flow rate. The lift begins to recover rapidly as the velocity increases. Recovery is not as rapid at higher mass flows and peaks out after the mass flow begins to decrease again. The suction pressure at the leading edge suffers the most disturbance during the surge cycle and is used as the key for fluctuation in lift.

The steady-state blade distribution is within one percent of the

maximum value of that obtained during surge. This correlation suggests that for this system the compressor approaches the quasisteady operating point as the mass flow rate is decreasing during the surge cycle.

The analysis of the stability of a fixed plenum volume compressor system shows that a compressor system can be unstable at large values of the parameter B, corresponding to a large plenum volume, if the compressor is operating on the positively sloped-portion of its characteristic. The time response of the system has some effect on the stability of the system. Fast response of a compressor to changes in mass flow rate tends to decrease the minimum value of B at which an instability first exists.

The instability obtained with the flexible plenum top in the experimental system could not be modeled well with a spring mass system for the range of springs tried. Explicit determination of the actual nonlinearity of such a spring is too involved to warrant further investigation at this time.

CONCLUSIONS

The rotor blade pressure distributions have been experimentally determined during surge of a low-speed axial-flow compressor for one throttle setting. The operation of the compressor system during surge has been determined for the same throttle setting and the two sets of results correlated to their point of occurance in the surge cycle. These measurements have been compared to the steady-state blade pressure distribution and system operating point.

An analytical model applied to a compressor system operating on The positively-sloped portion of the compressor characteristic showed that the system becomes unstable at large plenum volumes. A dependence of the system stability on the time response was determined from the same analytical model.

The use of a flexible plenum top in an experimental compressor system has allowed surge of the system similar to classical surge to be obtained for a much smaller plenum volume than normally required. A major difficulty encountered with this system was the oscillation superimposed on the mass flow rate and plenum pressure normally exhibited in surge. This is due to the natural resonance of the spring mass system associated with the flexible plenum top.

RECOMMENDATIONS

The results of this experiment suggest several areas of further study that are pertinent to a better understanding of surge. These areas should include the following:

- A study of the surge cycle as the throttle position is changed along the stalled region of the compressor map, including the rotor blade pressure distributions and the system operation path;
- Investigation of the effect the slope of the compressor characteristic has on the system geometry necessary to prevent surge;
- Development of a method of determining the response time of the compressor to changes in mass flow;
- A study similar to the one presented here using a large fixed plenum volume;
- A study of rotor blade pressure distributions during surge of a high-speed axial-flow compressor using an available FM telemetry system for transmission of rotor blade pressures from the rotor to stationary instrumentation.

LITERATURE CITED

1. Bullock, Robert O., Ward W. Wilcox, and Jason J. Moses, Experimental and Theoretical Studies of Surging in Continuous Flow Compressors", NACA Report No. 861, 1946.

2. Binder, R. C., "A Study of Surging in Fan or Compressor Systems", Journal of the Franklin Institute, Feb. 1946, pp. 125-136.

3. Pearson, H., and T. Bowmer, "Surging of Axial Compressors", The Aeronautical Quarterly, Vol. 1, Nov. 1949.

4. Pearce, R. B., "Causes and Control of Powerplant Surge", Aviation Weekly, Vol. 52, No. 3, Jan. 16, 1950, pp. 21-25.

5. Bullock, R. O. and H. B. Finger, "Compressor Surge Investigated by NACA", Society of Automotive Engineers Journal, Vol. 59, No. 9, Sept. 1951, pp. 42-45.

6. Foley, John R., "Compressor Surge Topic at SAE Round Table", Society of Automotive Engineers Journal, Vol. 59, No. 9, Sept. 1951, pp. 46-50.

7. Huppert, M. C., and W. A. Benser, "Some Stall and Surge Phenomena in Axial Flow Compressors", Journal of Aeronautical Science, Vol. 20, No. 12, Dec. 1953, pp. 835-845.

8. Pearson, C. E., "A Study of Surge in Compressors and Jet Engines", Journal of the Aeronautical Sciences, Vol. 22, No. 1, Jan. 1955, pp. 10-16.

9. Emmons, H. W., C. E. Pearson, and H. P. Grant, "Compressor Surge and Stall Propagation", Transactions of the ASME, Vol. 77, April 1955, pp. 455-469.

10. Pearson, C. E., "Surge Behavior in a Three-Stage Compressor", Journal of the Aeronautical Sciences, Nov. 1955, pp. 799-802.

11. Lubick, R. J. and L. E. Wallner, "Stall Prediction in Gas-Turbine Engines", Journal of Basic Engineering, Transactions of the ASME, Vol. 81/D, Sept. 1959, pp. 401-407.

12. Howell, W. T., "Stability in Axial Compressors", The Aeronautical Quarterly, Vol, XV, Nov. 1964, pp. 328-356.

13. Pearson, H., "A Contribution to the Analysis of Axial Flow Compressor Characteristics", Aeronautical Quarterly, Vol. XV, Feb. 1964, pp. 39-52.

14. Huppert, M. C., "Compressor Surge", Chapter XII of "Aerodynamic Design of Axial Flow Compressors", NASA SP-36, 1965.

15. Kuhlberg, J. F., D. E. Sheppard, E. O. King, and J. R. Baker, "The Dynamic Simulation of Turbine Engine Compressors", Fifth Propulsion Joint Specialist Conference, Colorado, 1969, AIAA, No. 69-486.

16. Willoh, R. G. and K. Seldner, "Multistage Compressor Simulation Applied to the Prediction of Axial Flow Instabilities", NASA TM-X-1880 1969, (NASA Cleveland, Ohio)

17. Corbett, A.G. and R. L. Elder, "Stability of an Axial Flow Compressor with Steady Inlet Conditions", Journal of Mechanical Engineering Science, Vol. 16,No. 6, Dec., 1974, pp. 377-385.

18. Greitzer, E. M., "Surge and Rotating Stall in Axial Flow Compressors Part I: Theoretical Compression System Model", Journal of Engineering for Power, Transactions of the ASME, April 1976, pp. 190-198.

19. Greitzer, E. M., "Surge and Rotating Stall in Axial Flow Compressors Part II: Experimental Results and Comparison with Theory", Journal of Engineering for Power, Transactions of the ASME, April 1976, pp. 199-217.

20. Schultz, P. E., "Pressure Distribution on a Rotating Axial-Flow Compressor Blade", M.S. Thesis, Virginia Polytechnic Institute and State University, 1976.

21. Weick, Fred E., Aircraft Propeller Design, McGraw-Hill Book Co., Inc., New York, 1930.

APPENDIX A

Frequency Response of Scanivalve

To qualify the method of data acquisition for the on-rotor blade pressure distribution, the frequency response of the Scanivalve system was required. A fluidic system was used to impose a pressure signal on the Scanivalve system at the rotor blade total-pressure port. A high-response Kulite pressure transducer, model CQH-152-15D, was used to monitor the input pressure. The input wave was generated by rotating a slotted disk through an interruptable jet. An AC motor regulated by a variac was used to vary the wave frequency. A two-channel storage oscilloscope was used to monitor and record the pressure wave amplitude and frequency at the input and output. Due to the nonlinearity of the wave generation system, the input wave was not perfectly square. Spikes and overshoots below the zero pressure level were neglected since their corresponding frequency was well above the range of interest. Those spikes above the steady-state input level were also neglected for the same reason. An amplitude versus frequency plot for maximum steady-state positive pressures of 1.0 and 2.0 kPa (4.0 and 8.0 in. H_2O) are given in Figs. A1 and A2. The amplitude ratio remains constant at 100 percent from 0 through 5 Hz. At 10 Hz it has dropped to 95 percent and beyond 10 Hz it drops off sharply. The frequency of surge is on the order of 1 Hz. This is well within the response range of the Scanivalve system.

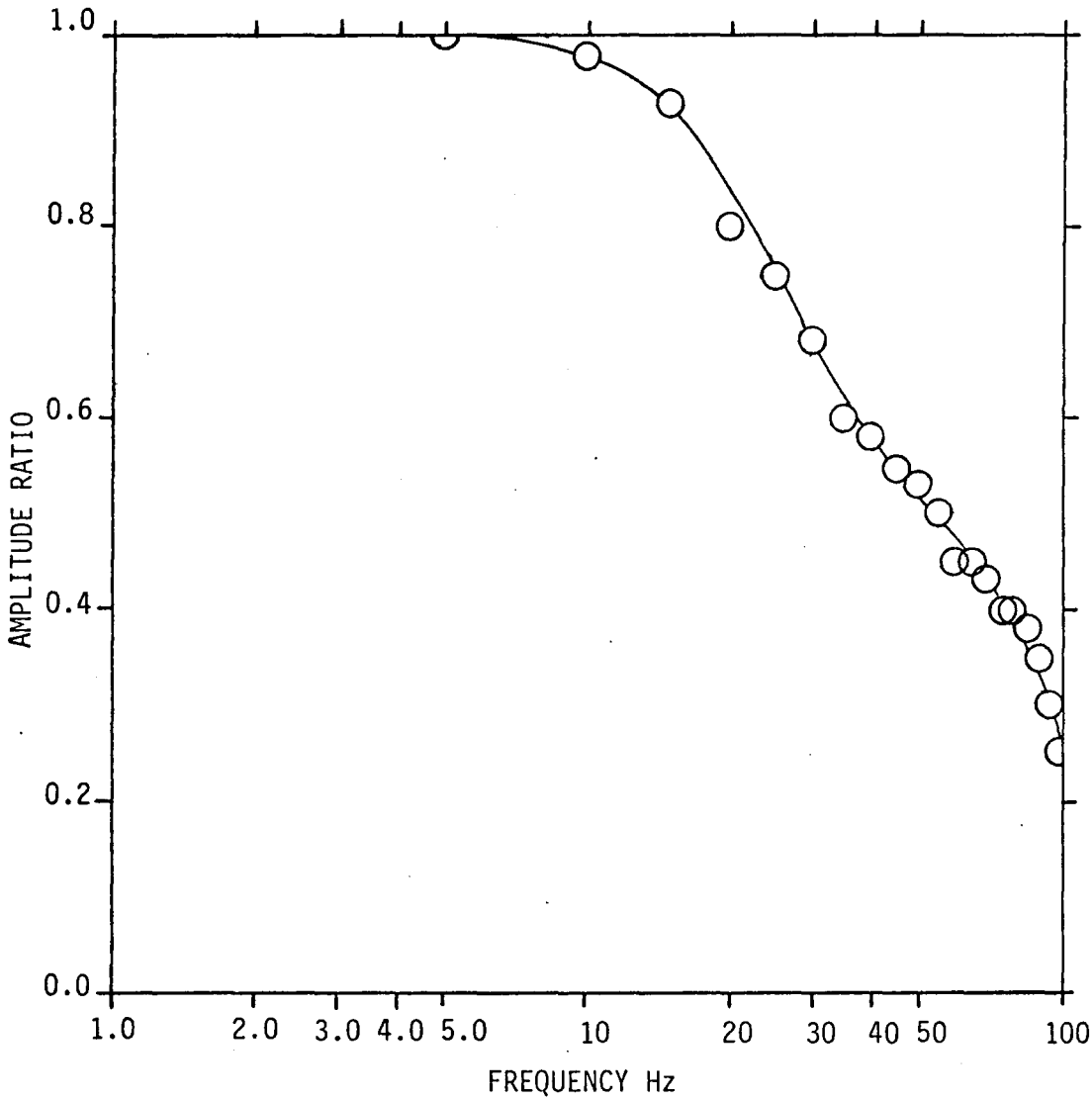

FIGURE A1. FREQUENCY RESPONSE OF SCANIVALVE - INPUT OF 1 kPa

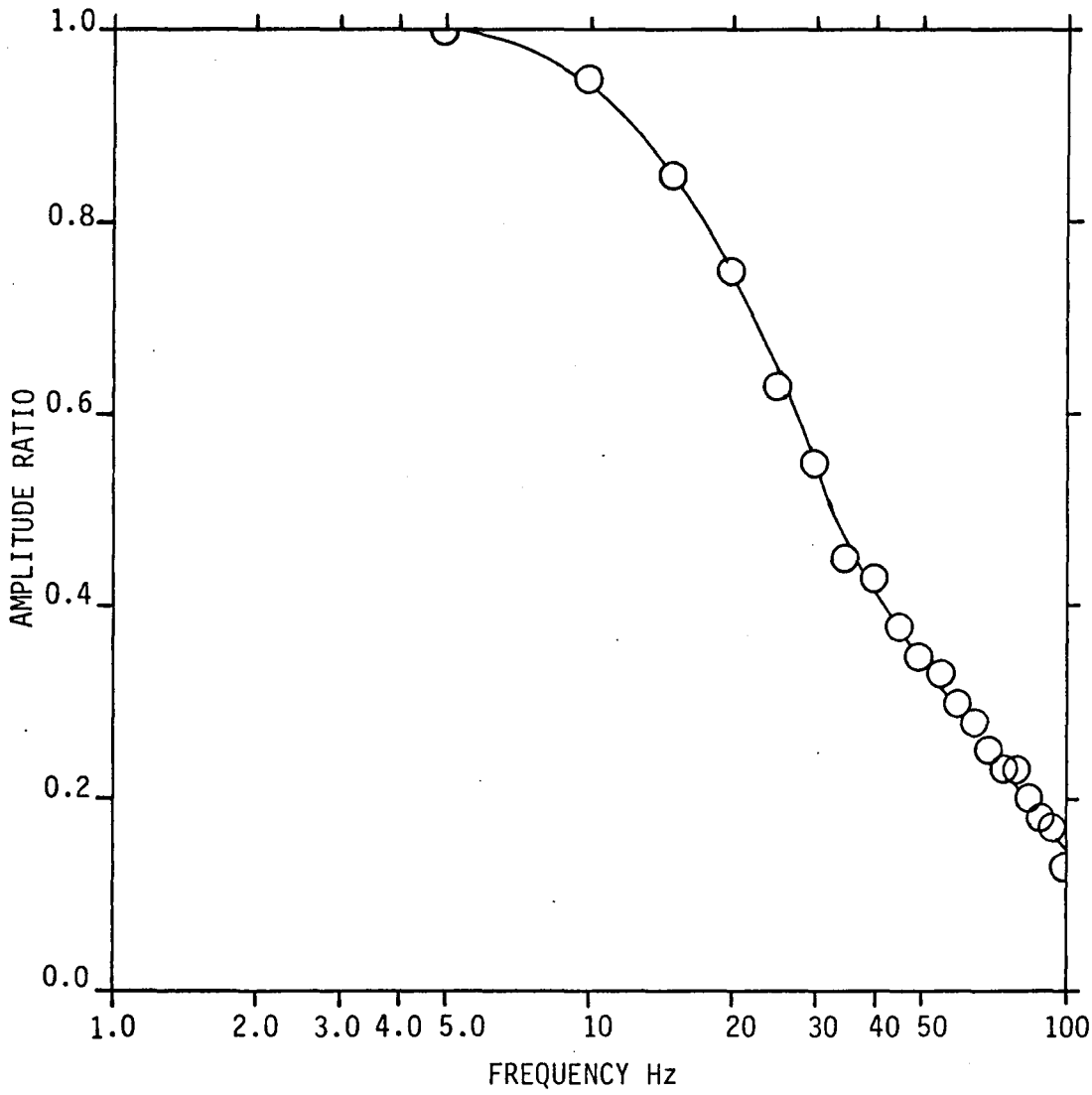

FIGURE A2. FREQUENCY RESPONSE OF SCANIVALVE - INPUT OF 2 kPa

The vita has been removed from the scanned document

BLADE PRESSURE DISTRIBUTIONS DURING SURGE OF A LOW-SPEED AXIAL-FLOW COMPRESSOR

by

Clifford Thomas Jones

(ABSTRACT)

An investigation of rotor blade pressure distributions at three span positions during surge of a low-speed axial-flow compressor was conducted for a single throttle position. The operating path of the compressor system was experimentally determined and the blade pressure distributions were correlated to their point of occurance during the surge cycle.

A comparison of these pressure distributions with the blade pressure distributions obtained during steady-state operation of the compressor at the same throttle position is presented. The steady-state compressor characteristic was determined to show the range of operation of which the compressor was capable.

A mathematical model was applied to the experimentally-determined compressor characteristic and the system geometry varied to determine its effect on the stability. The effect of the time response of the compressor, to changes in mass flow rate, on the stability of the system was also investigated.